Climate Dynamics (2023) 61:5309–5330
https://doi.org/10.1007/s00382-023-06857-w

Continental configuration controls the base-state water vapor greenhouse effect: lessons from half-land, half-water planets

Marysa M. Laguë[1,2] · Gregory R. Quetin[3] · Sarah Ragen[4] · William R. Boos[5,6]

Received: 28 October 2022 / Accepted: 5 June 2023 / Published online: 23 June 2023

Abstract

The distribution of land and ocean on Earth's surface shapes the global atmospheric circulation and climate by modulating fluxes of water and energy between the surface and the atmosphere. Here we rearranged land in an idealized climate model to explore the effect of eight simplified continental configurations on global climate, finding several counterintuitive results. The limited capacity of land to hold water and the smaller heat capacity of land compared to ocean—rather than surface albedo differences—are the primary drivers of continental control on global mean temperature. Specifically, the presence of land in certain locations can enhance tropospheric water vapor content, increasing the greenhouse effect and clear-sky shortwave absorption; these effects can warm the planet more than the cooling effect of higher land surface albedos. For example, continental configurations with land in polar regions and large tropical oceans have the warmest, wettest global climates. Configurations with large tropical land masses are not hot desert planets, but have the coolest global climates due to reduced evaporation and thus reduced atmospheric water vapor compared to configurations without land in the tropics. Interactions between the small heat capacity of land and the seasonal cycle can lead to certain continental configurations having even warmer, wetter atmospheres than an aquaplanet. Our results demonstrate that different configurations of land, such as those obtained through past tectonic movement or on rocky exoplanets, set planetary climate through mechanisms beyond those involving surface albedo or orographic effects.

Keywords Water vapor · Climate · Continents · Land–atmosphere interactions

1 Introduction

The distribution of continents on Earth's surface alters both terrestrial and global climate in myriad ways: by modulating surface-atmosphere exchange of water and energy, shaping atmospheric circulation patterns, and delineating ocean basins. Despite its importance, the fundamental role of continental distribution in setting Earth's base-state climate remains poorly understood. In this study, we explore how the distribution of land on Earth's surface alters global evaporation patterns and water vapor concentrations, with implications for global mean surface temperatures and climate.

Physical differences between the land and the oceans alter the way the overlying atmosphere interacts with either surface. The land tends to be brighter, drier, rougher, and have a lower heat capacity than the ocean (Budyko 1961, 1969; Payne 1972; Bonan 2008; Jin et al. 2004; Wiscombe and Warren 1980; Sud et al. 1988; Cess and Goldenberg 1981; North et al. 1983). Oceans can redistribute energy in the climate system by moving heat laterally while the land

✉ Marysa M. Laguë
marysa.lague@utah.edu

1 Coldwater Lab, Center for Hydrology, University of Saskatchewan, 1151 Sidney Street, Unit 116, Canmore, AB T1W 3G1, Canada

2 Department of Atmospheric Sciences, University of Utah, 135 S 1460 E, Room 819, Salt Lake City, UT 84112-0102, USA

3 Department of Geography, University of California, Santa Barbara, 1832 Ellison Hall, Santa Barbara, CA 93106-4060, USA

4 School of Oceanography, University of Washington, 1501 NE Boat St, Seattle, WA 98195, USA

5 Department of Earth and Planetary Science, University of California, Berkeley, 307 McCone Hall, Berkeley, CA 94720-4767, USA

6 Climate and Ecosystem Sciences Division, Lawrence Berkeley National Lab, 1 Cyclotron Rd, Berkeley, CA 94720, USA

cannot (Loft 1918; Richardson 1980; Ferrari and Ferreira 2011). Additionally, while water for evaporation is effectively unlimited in the oceans, the availability of water for evaporation to the atmosphere varies widely over different land regions as a function of the local climate (Baldocchi et al. 1997). Terrestrial evaporation and the surface supply of water varies seasonally and behaves differently under different climates. Moreover, while the evaporation from the ocean is governed by atmospheric inputs (i.e. wind speed and radiation), the evaporation from the land surface also varies with soil moisture and physical properties of soil and vegetation that provide resistance to terrestrial evaporation (Manabe 1969; Bonan 2008).

In slab ocean aquaplanet simulations, the organization of tropical rainfall, the location of the extratropical jet, and the strength of the Hadley circulation are all shown to be impacted by changes in atmospheric water vapor, sea surface temperature, and solar insolation (Kirtman and Shukla 2000; Barsugli et al. 2005; Kang et al. 2008, 2009; Voigt et al. 2014). The influence of continental configuration on atmospheric water vapor remains largely unexplored; however, recent work has shown that changes in terrestrial evaporation can drastically alter global-scale climate by modifying the total amount of atmospheric water vapor, a strong greenhouse gas (Laguë et al. 2021). In addition, other aquaplanet studies with dynamical oceans illuminate the connection between the distribution of meridional boundaries in the ocean and meridional heat transport, demonstrating how different climates can develop as a result of continental distribution (Enderton and Marshall 2009; Ferreira et al. 2010).

In the modern continental configuration, changes in land surface properties generate large changes in both surface climate and global-scale circulation (Shukla and Mintz 1982; Charney et al. 1975; Davin et al. 2010; Laguë et al. 2019). Moreover, the complex orography of mountain ranges impacts atmospheric circulation and generates large climate impacts over both land and ocean regions (Queney 1948; Eliassen and Palm 1960; Manabe and Terpstra 1974; Held 1985; McFarlane 1987; Held et al. 2002; Maroon et al. 2015; White et al. 2017). While this study focuses on the impact of continental distribution on temperatures, the impact of the location and size of continents on rainfall has been explored extensively in monsoon literature (Dirmeyer 1998; Yasunari et al. 2006; Maroon and Frierson 2016; Zhou and Xie 2018; Hui and Bordoni 2021). Continental extent also modulates the response of precipitation to reduced terrestrial evaporation (Pietschnig et al. 2021).

Idealized modelling studies have further explored how the distribution of land impacts temperature by allowing for albedo feedbacks (Barron et al. 1984) as well as by altering the rate of CO_2 weathering and thus the strength of the CO_2 greenhouse effect (Worsley and Kidder 1991). Latitudinal variations in albedo are driven directly by land distribution and indirectly through impacts on clouds and sea-ice (Enderton and Marshall 2009; Voigt et al. 2014). The temperature at each latitude is largely modulated by the meridional heat transport (Pierrehumbert 2010). Previous theory argues that heat transports by both the atmosphere and ocean, in turn, are largely insensitive to details of the dynamics responsible for the transport of heat, but rather depend more strongly on the mean planetary albedo and the equator to pole albedo gradient (Stone 1978; Enderton and Marshall 2009) as well as the evaporation and condensation of water (Fajber and Kushner 2021).

The role of land distribution in modulating global climate has implications for improving our understanding of climate in Earth's geologic past. Reconstructions of Earth's continental configuration over the last several hundred million years span a wide range of continental distributions, sometimes with land clustered into supercontinents, sometimes with land spread widely across the globe as in the modern era (Merdith et al. 2021). Simulations of paleoclimate include continental configurations vastly different to that of the modern world to study the transition between glacial and interglacial periods (Hoffman and Schrag 2002; Hoffman et al. 2017; Voigt et al. 2012), mass extinction events (Penn et al. 2018), and climatic changes due to the opening and closing of oceanic gateways (Straume et al. 2020).

We also expect to see different land arrangements on other planets. The habitability of exoplanets is a topic of interest to the astrobiology community (Méndez et al. 2021). The search for planets in the habitable zone hinges on locating the distance from a star that would allow for the presence of liquid water on a planet (a liquid environment is an expected requirement for life and water is the most abundant, common liquid in the universe) (Baross et al. 2007). While it is common to find exoplanets within the habitable zone of a star (Burke et al. 2015), whether or not those planets are actually habitable is difficult to determine (Kite and Ford 2018). Planets with a vast range of masses, sizes, and orbits have been detected (Seager 2013), with an anticipated wide range of variability in atmospheric mass and composition; the surface properties of those planets further modulate the planet's habitability (Rushby et al. 2020). The presence of liquid water is often used to determine the habitability of a planet (Seager 2013); however, the distribution of hospitable surface climates across a planet will depend on local surface climate.

In this study, we explore and compare the climates of eight Earth-like planets, which differ only in their continental configuration. Land differs from ocean in the simulations presented here in three key ways: it has a higher albedo; it has a smaller heat capacity; and it has a limited capacity to hold and evaporate water, with increased resistance to evaporation when the land is not saturated. These differences alter the fluxes of water and energy between the surface and the atmosphere over land vs. ocean, leading to changes in both local surface climate and global-scale climate.

We show that the distribution of continents exerts a fundamental control on global climate, even in a model without full representation of the differences between land and ocean. We investigate how the distribution of land and ocean alter planetary surface albedo, total absorbed shortwave radiation at the surface, atmospheric water vapor and the water vapor greenhouse effect, and atmospheric feedbacks resulting from differences in land vs. ocean heat capacity. We conclude with a discussion of the role of land in modulating the base-state climate of a planet, as well as the sensitivity of that climate to changes in terrestrial evaporation.

2 Methods

2.1 Model

In this study, we use Isca (Vallis et al. 2018), an idealized global circulation model (GCM) to explore the climate of an Earth-like planet with various idealized continental configurations. There is a seasonal cycle in insolation (23.439° obliquity, 0 eccentricity) over a 360-day year. All simulations have atmospheric CO_2 fixed at 300 ppm. The model is run using a T42 horizontal grid (∼ 2.8°) and 40 vertical levels.

The atmosphere uses moist dynamics and produces precipitation, but does not represent the radiative effects of clouds. Therefore, we set the surface albedo of both water and land to a higher value than in a model that represents clouds, allowing for a more reasonable planetary albedo at the top of the atmosphere (see below for more details). In the configuration of the model used here, there are no albedo feedbacks from snow on land or sea ice. The Rapid Radiative Transfer Model (RRTM) (Vallis et al. 2018; Clough et al. 2005; Mlawer et al. 1997) is used for atmospheric radiative transfer, and we use the Simple Betts–Miller convection scheme (Betts 1986; Betts and Miller 1986; Frierson 2007).

Analysis is primarily conducted using the Python programming language (Van Rossum and Drake 2009), particularly with the NumPy (Harris et al. 2020), SciPy (Virtanen et al. 2020), and xarray (Hoyer and Hamman 2017) packages.

2.2 Experiments

We run eight simulations, ranging from an all-ocean (Aqua) to an all-land (LandWorld) planet (Fig. 1). For five of the simulations, 50% of the planet's surface is covered by different distributions of land, and ocean covers the remaining 50% of the surface. TropicsLand has a single large continent in a belt around the equator, from 30° S to 30° N, with two oceans over each polar cap. CapLand is the inverse of this, with two continents capping the poles to 30° N/S, and a single large tropical ocean. NorthLand has a single large continent covering the whole northern hemisphere of the planet. EastLand has a single large continent covering the planet from the south to north poles, but only from 0–180° E longitude. In MeshLand, gridcells alternate between land and ocean in a checker-board pattern. Each patch of land/ocean in MeshLand is a single gridcell (roughly 2.8°). All simulations except RealLand have no orography. The RealLand simulation uses a semi-realistic, simplified continental configuration with roughly 20% of the surface covered by land, and idealized orographic representations of the Tibetan Plateau and the Rocky Mountains. This continental configuration is a modified version of that in Saulière et al. (2012), and is produced using Isca's idealized land generator function (Vallis et al. 2018).

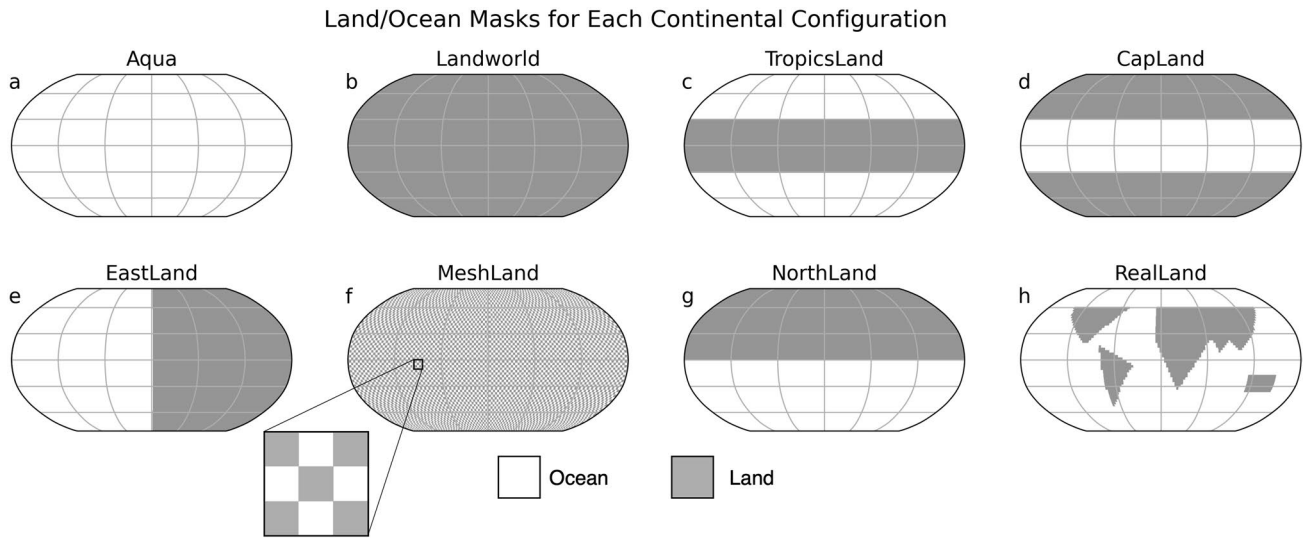

Fig. 1 Land/ocean masks for each continental configuration. Ocean is shown in white; land is shown in grey. A small section of MeshLand (f) is enlarged to show the land/ocean tiling pattern, where each tile is one gridcell (at roughly 2.8° resolution)

Land differs from ocean in these simulations through its albedo, smaller heat capacity, fixed capacity to hold water, and increased resistance to evaporation under dry soil conditions (Table 1). In our simulations, land is 1.3 times brighter than the ocean; the ocean has an albedo of 0.25 and the land an albedo of 0.325. This is brighter than typical albedo values for ocean (Jin et al. 2004) and (snow-free) land (Bonan 2008), allowing the model to generate similar global mean surface temperatures to our modern climate without the radiative effects of clouds, which increase planetary albedo (Herman et al. 1980).

The land can hold up to 150 mm of water at each point, with soil moisture represented by bucket hydrology. Land is initialized with 100 mm of water at every land gridcell. When the bucket is less than 3/4 full, the evaporative resistance of the land surface increases linearly as a function of soil dryness. When the bucket is more than 3/4 full, the resistance to evaporating water from the land surface is the same as that over open water. Water in excess of the bucket capacity is discarded as runoff; in effect, it is immediately returned to the ocean. However, in LandWorld there is no ocean for runoff to be discarded to, nor is there an oceanic water source to replenish the atmosphere with water; thus, discarding runoff would result in a system that does not conserve water. To address this, hydrology on LandWorld is modified to allow for the formation of lakes: water is allowed to accumulate in excess of the 150 mm bucket capacity, with the evaporative resistance the same as that of open water until the amount of water in the gridcell drops back below 150 mm, at which point the standard bucket hydrology rules apply. The atmospheric circulation of LandWorld rapidly transports all of the available moisture to the polar regions where the land forms two "lakes" (see Laguë et al. 2021 for discussion of the formation of polar lakes on an all-land planet). Note that despite the implementation of lakes in the LandWorld simulation, there is still a slow leak of water vapor from the atmosphere which causes the simulation to cool over time (Fig. 12); this is a known bug of Isca that is apparent in all-land configurations (see https://github.com/ExeClim/Isca/issues/177) and is not evident in the other simulations which can continuously replenish water vapor from the oceans.

The aerodynamic roughness of the land and ocean are the same in these simulations because the effects of surface roughness are outside the focus of this study. In reality, land is typically more aerodynamically rough than the ocean; the implications of this for climate are explored by past studies (Sud et al. 1988; Davin et al. 2010; Laguë et al. 2019).

Table 1 Surface properties of land vs. ocean in all simulations

	Albedo	Capacity to hold water (mm)	Heat capacity in equivalent water depth (m)
Ocean	0.25	Unlimited	20
Land	0.325	150[a]	2

[a]Except in the LandWorld simulation, where water is allowed to accumulate beyond 150 mm

The ocean is represented with a 20 m deep mixed layer ocean that allows sea surface temperatures to evolve. No lateral heat transport is prescribed in these simulations. The heat capacity of the land surface in these simulations is 1/10 that of the ocean, and corresponds to that of a 2 m deep mixed layer ocean, a larger value than the heat capacity of typical land surfaces on the modern Earth. The land and ocean heat capacities were selected based on previous Isca simulations that generate realistic climatologies (Thomson and Vallis 2019; Geen et al. 2018).

Simulations are run for 20 years, with the first 4 years discarded to allow for model spin-up. After 4 years, global mean surface temperatures and average terrestrial soil moisture are stable for all simulations except LandWorld, which continues to lose water and cool throughout the length of the simulation (Fig. 12 in Appendix A). Over the last decade of the LandWorld simulation, global mean temperatures decrease by roughly 1.5 K, but even without the water leak we expect this simulation to be cold and dry because the atmospheric circulation rapidly transports all the moisture to the polar regions where there is limited energy for evaporation.

3 Results and discussion

3.1 Overview of scenarios

The eight different continental configurations considered here generate a wide variety of climates. The global average annual mean surface temperatures span almost 15 K (Fig. 2), ranging from the coldest global mean surface temperature on LandWorld (273.0 (± 1.2) K) to the warmest global mean surface temperature closely shared among RealLand (286.7 (± 0.03) K) and CapLand (286.5 (± 0.1) K; numbers in brackets show ± the interannual standard deviation).

Over paleoclimate timescales, global mean temperatures are influenced by many factors, including changes in atmospheric CO_2 and ocean heat transport (Tierney et al. 2020). Our results show that continental distribution—independent of its impacts on CO_2 or ocean circulation—could be a potentially overlooked contributor to variations in past climate, as the range of surface temperatures generated solely by altering the continental arrangement and total amount of land produces changes in global mean surface temperature of the same order of magnitude as the temperature range experienced on Earth over the last 500 million years (Voosen 2019).

The spatial distribution of surface temperatures varies between simulations (Fig. 2). The strongest equator-to-pole annual mean difference in surface temperature

occurs over the continent in the NorthLand configuration, followed by LandWorld and CapLand, while the smallest equator-to-pole temperature difference occurs in both hemispheres of RealLand, followed by Aqua (Table 2).

Along with global temperature, the continental configurations also alter atmospheric circulation and global mean precipitation, with configurations with both more and less global mean rainfall than the modern Earth (Fig. 3). The highest global mean rain value occurs in the CapLand continental configuration (3.27 ± 0.01 mm/day), with the most rain falling over the tropical ocean. The lowest global mean precipitation values occur in Landworld (0.31 ± 0.16 mm/day).

All the continental configurations considered in this study can support liquid water, a common criteria for planetary habitability (Seager 2013). However, the total area of land that would be hospitable to modern terrestrial ecosystems varies substantially across these continental configurations. To coarsely quantify the total land area in each simulation hospitable to modern day terrestrial ecosystems, we calculate the land area in each simulation with the annual mean temperature above freezing ($T_{ANN} > 0\,°C$).

Table 2 Area in millions of km^2 (global and land-only) with annual mean temperature above 0 °C ($T_{ANN} > 0\,°C$), and with annual mean precipitation above 300 mm/year ($P_{ANN} > 300$ mm/year). Also shown is the % of the total land on each planet meeting these criteria, and the equator to pole temperature difference in K for each continental configuration (noted separately for the northern and southern hemispheres for NorthLand and RealLand, which are not symmetric about the equator)

Continental configuration	Total area with $T_{ANN} > 0\,°C$, in [km$^2 \times 10^6$]	Land area with $T_{ANN} > 0\,°C$, in [km$^2 \times 10^6$]	% of Land area with $T_{ANN} > 0\,°C$	Eq to pole Δ T [K]	Total area with $P_{ANN} > 300$ [mm/year], in [km$^2 \times 10^6$]	Land area with $P_{ANN} > 300$ [mm/year], in [km$^2 \times 10^6$]	% of Land area with $P_{ANN} > 300$ [mm/year]
Aqua	424	–	–	33	478	–	–
LandWorld	337	337	66	45	57	57	11
TropicsLand	378	260	100	34	273	64	25
CapLand	422	162	65	44	510	250	100
EastLand	396	193	76	43	322	85	33
MeshLand	416	205	80	36	492	244	96
NorthLand	406	188	74	46 (NH), 31 (SH)	432	189	74
RealLand	440	108	91	32 (NH), 29 (SH)	453	81	68

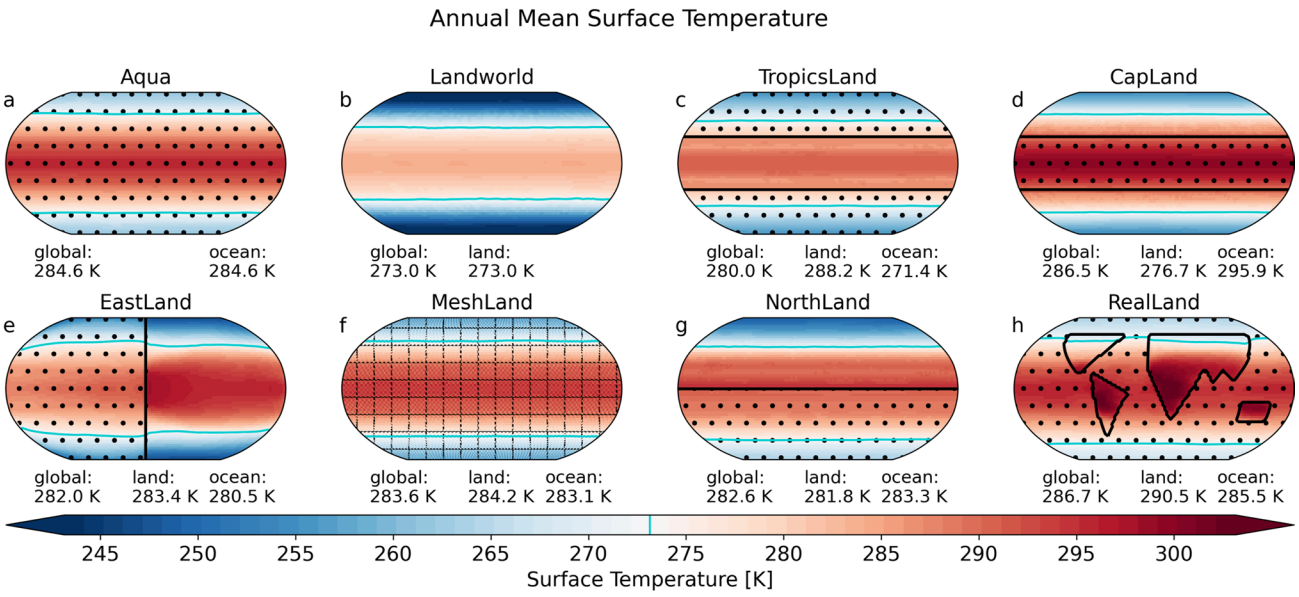

Fig. 2 Maps of annual mean surface temperature [K]. Ocean regions are stippled (except in MeshLand, where diagonal hatching is used to indicate the alternating land/ocean gridcells). Global, land-only, and ocean-only area-weighted annual mean values are noted below each map

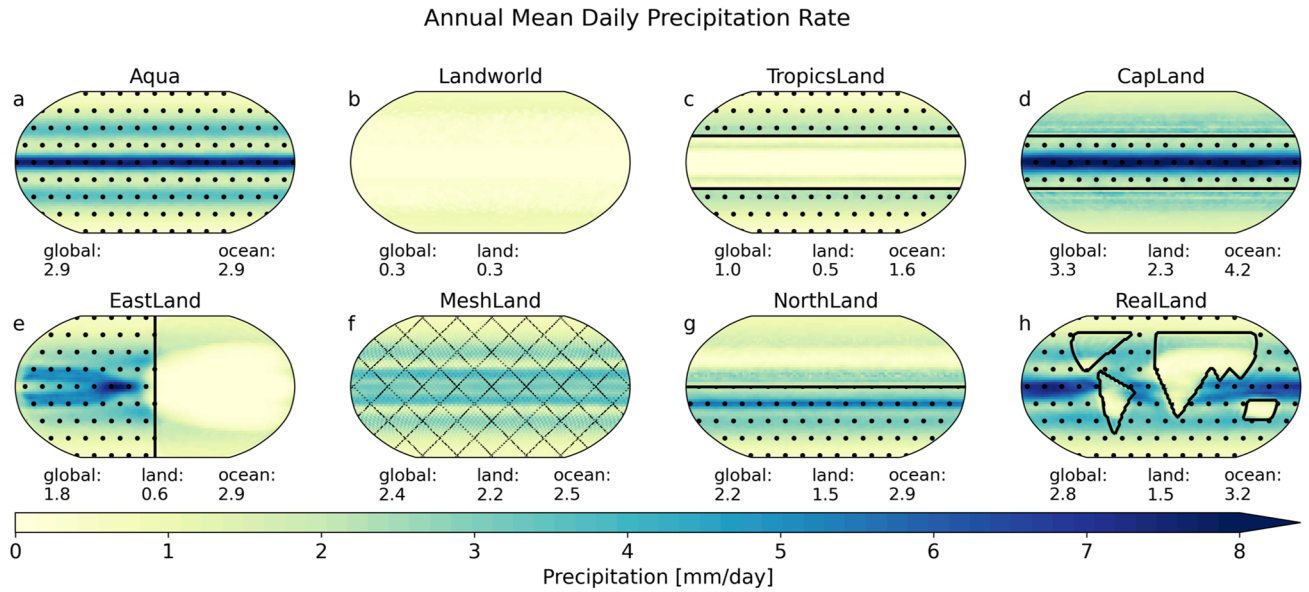

Fig. 3 Maps of annual mean precipitation [mm/day]. Ocean areas are stippled (except in MeshLand, where diagonal hatching is used to indicate the alternating land/ocean gridcells). Global, land-only, and ocean-only area-weighted annual mean values are noted below each map

We also calculate the land area with annual mean precipitation above 300 mm/year ($P_{ANN} > 300$ mm/year), which roughly marks the divide between arid and semi-arid ecosystems (Salem 1989).

The spread in the total land area with $T_{ANN} > 0\,°C$ across simulations spans hundreds of millions of square kilometers (Table 2). RealLand has the smallest total land with $T_{ANN} > 0\,°C$, but it also has the smallest amount of land to begin with. Of the 50/50 land/ocean planets, CapLand and NorthLand have the smallest land area with $T_{ANN} > 0\,°C$, while TropicsLand and MeshLand have the most. LandWorld, which has the largest total land area, also has the largest amount of land above freezing in the annual average. However, both LandWorld and TropicsLand have large expanses of very dry land (Table 2). Indeed, only 11% of the land on LandWorld and 25% of the land on TropicsLand have $P_{ANN} > 300$ mm/year. In contrast, 96% and 100% of the land in MeshLand and CapLand (respectively) exceed the 300 mm/year precipitation threshold. Climate zone classifications provide a combined estimate of temperature and precipitation impacts on ecosystem distribution; Köppen–Geiger climate zones for each continental configuration explored here, calculated following Kottek et al. (2006), are shown in the appendix in Fig. 13.

In the sections below, we examine the main drivers of this wide spread in surface temperatures across the various continental arrangements, with particular focus on how land distribution impacts surface evaporation and atmospheric water vapor, the role of albedo, and feedbacks driven by differences in land vs. ocean heat capacity. The appendices contain figures showing transient and seasonal adjustments, meridionally resolved details, and additional fields of interest.

3.2 Association of water vapor and the greenhouse effect with surface temperatures

The various continental configurations explored here have a strong control on surface evaporation, and thus on the concentration of atmospheric water vapor. We find that the impact of the continental configuration on water vapor is the dominant control driving the spread of global mean surface temperatures across simulations, while differences in albedo and absorbed shortwave radiation play a secondary role.

Continental configurations that allow for the largest globally averaged latent heat flux (evaporation) produce the warmest global mean surface temperatures (Fig. 4a). This contrasts with the intuition of evaporative cooling leading to cooler surface temperatures. There is a strong linear relationship ($r^2 = 0.87$) between the global mean values of surface temperature and surface latent heat flux. Configurations with high surface latent heat flux have high total column water vapor (Fig. 4b). However, given the temperature-dependence of water's saturation vapor pressure, we must further explore this relationship to understand the cause and effect.

The total amount and spatial distribution of water vapor, a strong greenhouse gas, varies substantially across the continental configurations explored here (Figs. 4b, 5). All other greenhouse gases are prescribed to be identical across the simulations. We assess the effect of differences in water vapor concentration by approximating the strength of the greenhouse effect (following Kiehl and Trenberth 1997) as the difference

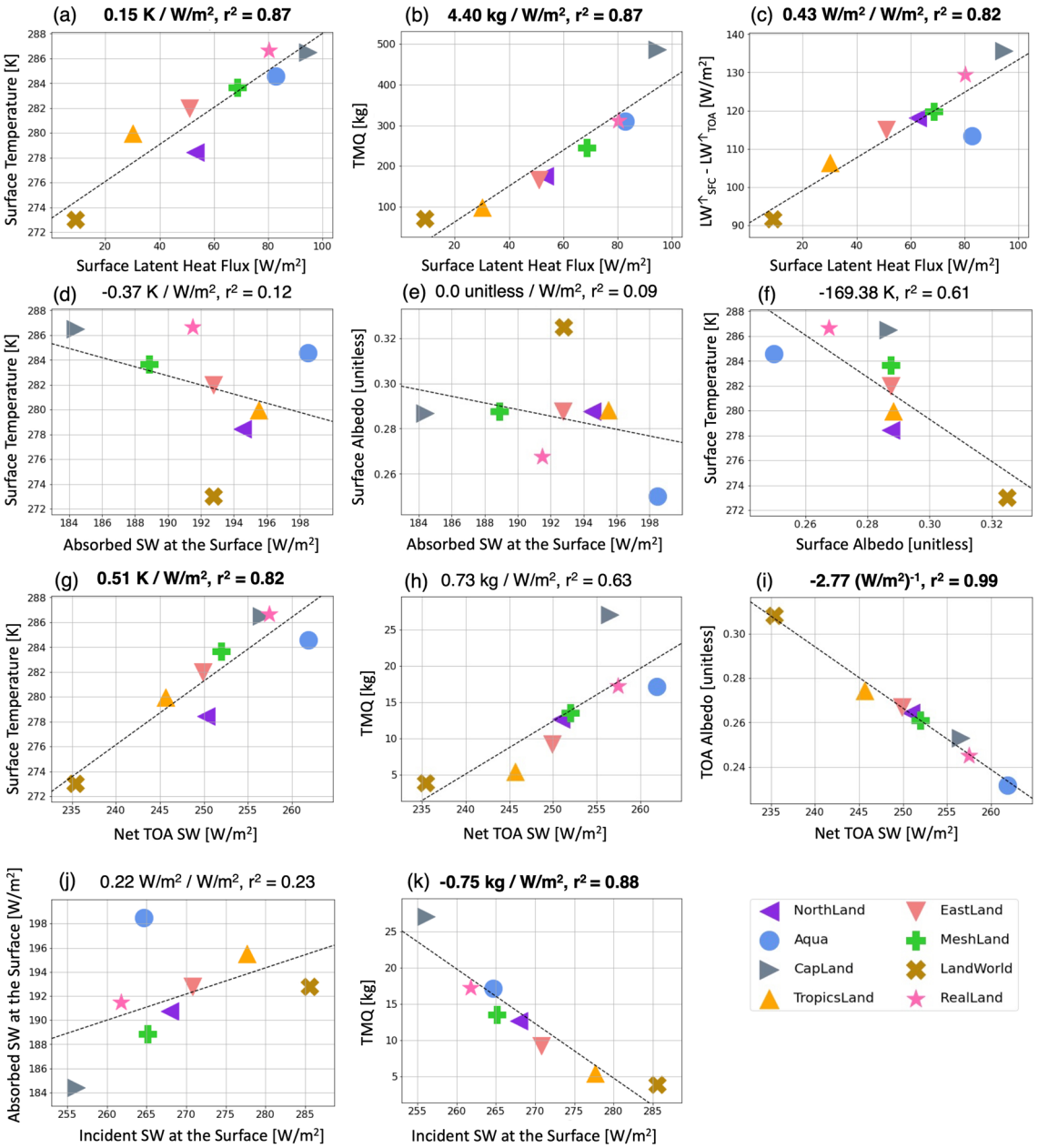

Fig. 4 Scatter plots showing the relationship between various global mean climate variables across the eight continental configurations. All values are shown for the annual mean, with each marker representing an individual continental configuration. The slope and r^2 value of a linear fit (dashed black line) is noted at the top of each panel, with slopes with a p-value < 0.05 shown in bold

between longwave (LW) radiation emitted at the surface and emitted at the top of the atmosphere (TOA; Eq. (1)):

$$LW_{diff} = LW^{\uparrow}_{surface} - LW^{\uparrow}_{TOA}. \quad (1)$$

Small values of LW_{diff} indicate a weak greenhouse effect while large values indicate a strong greenhouse effect.

Across the continental configurations tested, there are a wide variety of climate states that fall along a common line relating evaporation, water vapor, and surface temperatures. A strong linear correlation ($r^2 = 0.82$) exists across continental configurations between globally averaged latent heat flux and LW_{diff}, where configurations with high surface evaporation—and high water vapor (not shown)—have a stronger greenhouse effect (Fig. 4c). In the following sections, we discuss why each continental configuration leads to each distinct distribution of atmospheric water vapor and surface temperatures.

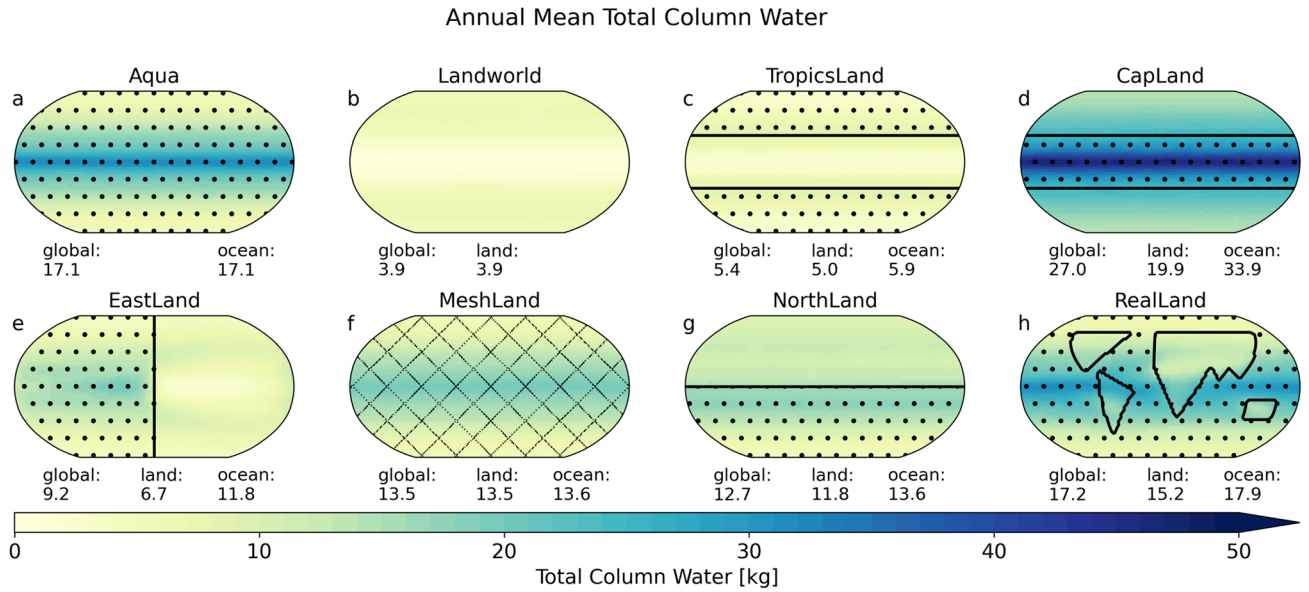

Fig. 5 Maps of climatological annual mean total atmospheric water vapor [kg] for each continental configuration. Ocean regions are indicated with black stippling, except in MeshLand where gridcells alternate between land and ocean (indicated by checkered hatching, which is not to scale with the model's grid). Global, land-only, and ocean-only area-weighted annual mean values are noted below each map

3.3 Surface albedo differences alone do not explain temperature spread

In our experimental planetary continental configurations, all planets that are 50% land and 50% ocean have the same globally averaged surface albedo. Yet, for the five continental configurations that are half land and half water and thus have identical surface albedos, there is a roughly 10 K spread in global mean surface temperature (Fig. 4e–g).

Planets with more water (Aqua and RealLand) have an overall darker surface while LandWorld has an overall brighter surface. Surface albedo determines how much of the shortwave radiation energy reaching the surface is absorbed at the planetary surface, and can play a role in controlling surface temperatures by modulating the total amount of energy available to the land surface. Because the model we use does not represent the radiative effects of clouds, we might expect surface albedo to have a stronger impact on top of atmosphere albedo—and thus climate—than in the modern Earth. However, we still see a large spread in the TOA albedo (as shown by the net shortwave radiation flux at the TOA; Fig. 4i), resulting from changes in water vapor.

Along with the surface albedo, the amount of incident shortwave radiation in a region also modulates how much shortwave radiation is available for absorption at the surface. Given the absence of clouds in our simulations, one might hypothesize for simulations with darker ocean near the tropics and brighter land near the poles to absorb more shortwave radiation than simulations with bright land in the tropics, since more shortwave radiation is incident at the top of the atmosphere in the tropics than in the high latitudes. However, we find simulations with bright tropical land masses, including TropicsLand and LandWorld, absorb relatively high amounts of shortwave radiation at the surface (Fig. 4d, e). This apparent discrepancy between surface albedo and absorbed shortwave radiation results from more shortwave radiation reaching the surface in configurations with tropical land (Fig. 4h). Water vapor impacts both shortwave and longwave radiative transfer through the atmosphere, and larger amounts of shortwave radiation reach the surface in TropicsLand and LandWorld because the atmosphere is very dry.

Top of atmosphere albedo plays a central role in modulating global climate (Donohoe and Battisti 2011). As our simulations do not have clouds, top of atmosphere albedo is instead a function of surface albedo and water vapor concentrations. The large differences in water vapor across our simulations generate a spread in TOA albedo even among simulations with the same globally averaged surface albedo (Fig. 4f; note that we plot absorbed SW at TOA as a proxy for TOA albedo because all models have identical insolation). There is a correlation ($r^2 = 0.82$) between the globally averaged TOA absorbed SW and global mean surface temperatures, with continental configurations which absorb more net SW radiation at the TOA being generally warmer than configurations which absorb less net SW radiation at the TOA. However, TOA albedo alone does not explain the full spread in surface temperatures across continental configurations. For example, Aqua absorbs the most TOA SW (i.e. has the lowest TOA albedo), but both RealLand and CapLand are warmer.

Though the largest difference in surface albedo is between Aqua and LandWorld, their difference in globally averaged shortwave radiation absorbed at the surface is fairly small (Fig. 4e). That is, globally averaged surface albedo does not correlate well with globally averaged absorbed surface shortwave radiation. While the surface in LandWorld is much more reflective than the surface in Aqua, the dry atmosphere in LandWorld allows a larger amount of solar energy to reach the surface than the moist atmosphere of Aqua (Figs. 4j, k, 5b). Atmospheric water vapor both scatters and absorbs shortwave radiation (even in the absence of clouds), leading to less shortwave radiation incident upon the surface of Aqua than the surface of LandWorld.

For the 50/50 land/water planets, which all have the same surface albedo, there is about a 10 W/m^2 range in total absorbed shortwave radiation (SW) at the surface (Fig. 4e). RealLand, which has a smaller total land area, falls roughly in the middle of the spread. The reason for this non-intuitive relationship between global mean surface albedo and global mean absorbed shortwave radiation at the surface is the result of variations in incident shortwave radiation at the surface between continental configurations, which are due to differences in atmospheric water vapor concentrations. For example, CapLand absorbs a relatively small amount of globally averaged shortwave radiation despite the presence of dark ocean surface in the tropics. However, CapLand has a large concentration of atmospheric water vapor in the tropics (Fig. 5d) due to its tropical ocean. Because atmospheric water vapor scatters and absorbs shortwave radiation, there is less shortwave radiation incident upon the dark tropical surface in CapLand than there is in simulations with drier atmospheres, and thus less shortwave radiation is absorbed despite the dark tropical surface (Fig. 4j). TropicsLand, in comparison, has a much more reflective tropical surface than CapLand, but absorbs more total shortwave radiation because its dry atmosphere allows more solar energy to reach the surface than the humid atmosphere of CapLand.

Over sufficiently long timescales, the surface must balance the absorption of shortwave energy either by heating up (and thus removing energy from the surface as longwave radiation or sensible heat), or by evaporating water (removing energy from the surface as latent heat). For land, this occurs on comparatively short time scales due to its small heat capacity. The larger heat capacity of the ocean allows it to absorb more shortwave energy before that energy must be shed as latent heat, sensible heat, or longwave radiation. This difference in heat capacity plays a critical role in explaining why CapLand is both warmer and wetter than Aqua, which we discuss in Sect. 3.6. In the real ocean, heat can also be transported by the ocean circulation, but our simulations have no ocean circulation by design. The sign of the relationship between the amount of shortwave radiation absorbed at the surface and the global mean surface temperature is the opposite of what one might naively expect: the warmest climates are those that absorb the least amount of SW radiation at the surface (Fig. 4d). Planets with less land (RealLand, Aqua) fall above this line, while the planet with more land (LandWorld) falls below this line.

LandWorld is colder than all the other continental configurations despite the large amount of absorbed SW at the surface (Fig. 4d). CapLand, RealLand, and Aqua span the full range of simulated globally mean absorbed shortwave at the surface, yet these three continental configurations are the 3 warmest planets, with similar global mean surface temperatures (roughly 285 K).

This disconnect between globally averaged surface albedo, absorbed SW at the surface, and surface temperature implies that we cannot rely on the surface albedo differences of land and water alone to explain the varied climates across continental configuration. These simulations do not allow for cloud effects on radiation; however, when cloud impacts on planetary albedo are taken into consideration for the modern Earth, surface albedo contributes only a small amount to the top of atmosphere albedo, which controls the total amount of energy absorbed by the Earth system at any given location (Donohoe et al. 2013).

3.4 Longitudinal distribution of land cools by limiting evaporation over the Eastland super-continent

The effect of continental arrangement on surface temperatures and climate through water vapor vs. albedo is further demonstrated in the comparison of MeshLand and EastLand. MeshLand and EastLand have the same amount of land at each latitude. As such, they have the same latitudinal distribution of surface albedo (or, equivalently, the same insolation-weighted surface albedo). We find that differences in water vapor driven by differences in evaporation are the dominant control making MeshLand a warmer planet than EastLand.

Despite MeshLand and EastLand having the same latitudinal distribution of surface albedo, there is more shortwave radiation incident upon the surface in Eastland, so more shortwave radiation is absorbed at the surface of EastLand compared to Meshland (Fig. 6). If this were the dominant control on surface climate, we would expect EastLand to be warmer than MeshLand. Instead, we see that MeshLand is warmer; this is a result of differences in the strength of the water vapor greenhouse effect between the two continental configurations.

The atmosphere in MeshLand has easy access to water everywhere, as each land gridcell is adjacent to ocean. In contrast, the atmosphere over the continent in EastLand is quite dry (c.f. Figs. 5e, f, 14e, f), particularly in the tropics where moisture that is advected onto the continent quickly precipitates out (Fig. 3e). The humid atmosphere of MeshLand results in a strong water vapor greenhouse effect, which drives the warmer temperatures of MeshLand compared to

EastLand. This difference in water vapor also explains the difference in incident shortwave radiation between the two simulations; however, as noted above, this difference in shortwave radiation is not the controlling factor on surface temperature differences between these simulations.

Each MeshLand "island" behaves most similarly to archipelagos like the Maritime Continent, where the surrounding ocean provides moisture and the islands provide vertical motion for rainfall (Kooperman et al. 2017). Meanwhile, the zonal extent of the super continent of EastLand limits the range of moisture transport for precipitation to the interior, similar to Earth's Asian continent (though more extreme). The resulting dry lands and overlying dry atmosphere of the EastLand super-continent cool the global climate.

In the idealized climate model used in these studies, there are no radiative effects of cloud cover. Cloud radiative effects are an important part of the climate system and can respond strongly to terrestrial processes (Cho et al. 2018; Sikma and Vilà-Guerau de Arellano 2019; Laguë et al. 2019; Kim et al. 2020), but they also represent a large source of uncertainty (IPCC 2013; Zelinka et al. 2017). While the radiative effects of clouds would play a role in the climate of all continental configurations considered here, they may be of particular importance in the comparison of MeshLand to EastLand. Specifically, we would expect MeshLand to be cloudy because its atmosphere has ample access to water everywhere and the smaller heat capacity of land would result in larger sensible heat fluxes over the land than the neighbouring ocean patches. This combination of vertical motion from sensible heating from the land and a steady moisture supply from both the ocean and the wet land would be conducive to the formation of cloud cover along the land/ocean boundary. The entire planet of MeshLand is comprised of patchy islands—areas which, on the modern Earth, enhance regional convection, cloud cover, and precipitation (Cronin et al. 2015), such as occurs near the Maritime Continent.

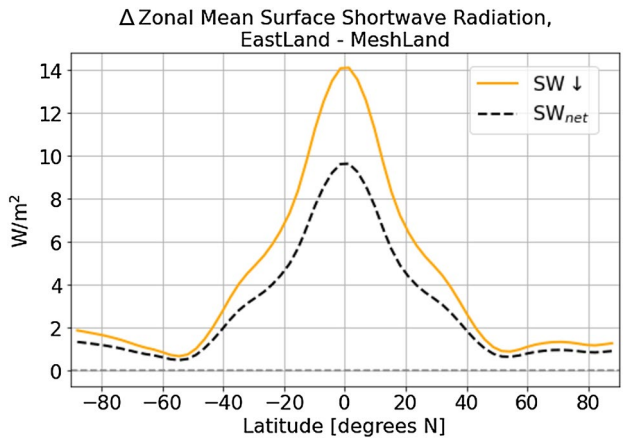

Fig. 6 Zonal mean, annually averaged difference in downwards (yellow) and net absorbed (black) shortwave radiation at the surface for EastLand–MeshLand

The patchy nature of MeshLand's continental distribution, and the resulting surface heat fluxes, is also reminiscent of regions of patchy deforestation in the tropics. In the Amazon, deforestation on the scale of tens of km^2 has been shown to lead to increased cloud cover at the grass-forest boundary. This deforestation generates regional circulations driven by sensible heating over the relatively dry grassland and moisture flux from the relatively moist rainforest (Khanna and Medvigy 2014). Further exploration of a MeshLand-like planet, potentially with land patches of varying size, in a model that allows for radiatively interactive cloud cover would be useful to explore the impact of coastal land on cloud formation at different latitudes.

Another process that strongly impacts cloud formation and precipitation over complex topography is orographic lift (Kirshbaum and Smith 2009; Houze 2012; Maroon et al. 2015). Elevated orography can drive circulations and alter free-tropospheric temperature and regional climate, but the physics of this are complex and interact strongly with surface albedo (Hu and Boos 2017). With the exception of RealLand, which has a simplistic representation of some mountain ranges, orographic effects are not represented in these flat-land simulations. Rather than exploring the orographic effects of continents on climate, here we are specifically focused on the differences in land vs. ocean heat capacity, albedo, and evaporative properties and their effect on climate.

3.5 Large tropical landmasses limit atmospheric water vapor

The coldest three simulations (LandWorld, Northland, and TropicsLand) all have relatively large amounts of tropical land cover. These simulations are colder than the others at most latitudes in the annual mean (Figs. 2 and 15). Even EastLand, in which half of the tropics are covered by land, is cooler and drier than the simulations with open water across the entire tropics. Land can affect the global water vapor concentration both through evaporation and by changing the saturation vapor pressure of the atmosphere through changes in air temperatures.

Albedo differences between land and ocean cannot explain why configurations with large tropical land masses are cooler than other configurations. As discussed in Sect. 3.3, the total amount of shortwave radiation absorbed at the surface is similar between these three simulations, and is higher than any other planet except Aqua (Fig. 4). Low shortwave radiation absorption over the tropical continents doesn't explain the cooler global temperatures—thus we examine differences in evaporation between simulations.

Generally, land is a dryer surface with limited water holding capacity compared to the ocean, and so serves to limit

evaporation over the continents. The evaporative demand of the atmosphere is high in the tropics because of the warmer tropospheric air driven by high insolation. When there is ocean in the tropics, this evaporative demand is supplied by an effectively infinite reservoir of surface water. However, when the tropics are covered with land, the water on the land is quickly evaporated. While some of this moisture initially rains onto the land surface, e.g. in a classic intertropical convergence zone that occupies a narrow range of latitudes, tropical moisture export events (e.g. see Knippertz and Wernli 2010) move moisture off the tropical continent. Eventually the tropical land of TropicsLand dries out except along the edges of the continent, which experience seasonal precipitation.

The large latitudinal extent of the continent (between 30 degrees N-S) inhibits near-surface atmospheric moisture transport into the continental interior from the polar oceans. That is, were the equatorial continent of a smaller latitudinal extent, the equatorward component of the trade winds would travel over ocean (evaporating water along the way) before making landfall, thus bringing moisture onto the continent. With a latitudinally wide tropical continent, the near-surface winds travelling equatorward lie over land, thus the air is much drier than if the wind was travelling over an ocean surface. This results in most of the TropicsLand continent being dry, which means the tropical atmosphere cannot evaporate a large amount of moisture from the surface, resulting in a dry tropical atmosphere (Fig. 16).

In the modern continental configuration, near-surface winds in the tropics move moisture equatorward. However, in TropicsLand, the subsiding branch of the Hadley cell doesn't extend beyond the polar edge of the continent except in local summer. A small amount of moisture is brought onto the continental edge in summer (Fig. 16), but for the most part, surface winds in the low latitudes in TropicsLand do not travel over the ocean surface and thus do not transport moisture equatorward. In equilibrium, the large tropical land masses considered in this study are very dry and serve as a cap to tropical evaporation (Fig. 7).

Limited evaporation also means less latent cooling of the land surface, which could warm these tropical continents. However, the reduction of the water vapor greenhouse effect causes the continents to stay cool year round. The atmosphere at all latitudes becomes depleted in atmospheric water vapor (Figs. 5, 14). Instead of the surface temperature rising without evaporation, the atmosphere, robbed of its main source of moisture by the land surface, drys out and drives surface cooling via a reduced greenhouse effect. The weak greenhouse effect from low atmospheric water vapor is evident in the smaller magnitude of downwelling LW radiation at the surface in TropicsLand, LandWorld, and over the continent in Northland (Fig. 17). The water vapor feedback that operates in response to an arbitrary radiative forcing is expected to further reduce surface temperatures, amplifying the cooling produced by the initial land-induced drying.

While there is ample water available for evaporation at higher latitudes—e.g. over the polar oceans in TropicsLand, from high-latitude soil moisture in NorthLand and Landworld, or from the southern hemisphere ocean in NorthLand—the lack of energy for evaporation at higher latitudes and horizontal mixing by the atmospheric circulation

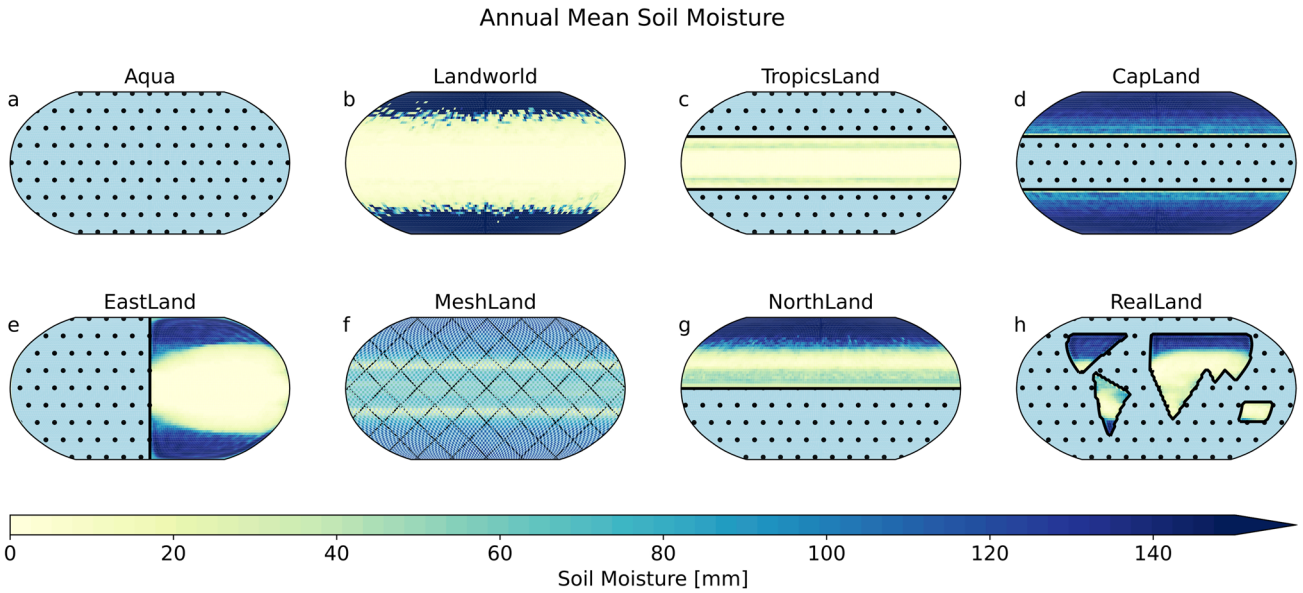

Fig. 7 Maps of annual mean soil moisture [mm]. Ocean areas are shown in light blue with stippling (except in MeshLand, where diagonal hatching instead of stippling indicates the alternating land/ocean gridcells). Note that all land regions have a maximum water-holding capacity of 150 mm except LandWorld, which has been modified to allow for lake formation to conserve water

together maintain a dry tropical atmosphere in these simulations. The mid-to-high latitude atmosphere in TropicsLand does not contain nearly as much water vapor as the Aqua, CapLand, MeshLand, or RealLand continental configurations (Figs. 5 and 14). The southern hemisphere in NorthLand has much more water vapor than the northern hemisphere, which is consistent with the warmer surface temperatures of the southern hemisphere. The tradeoff between surface warming from reduced evaporation and large-scale surface cooling from a reduced atmospheric water vapor greenhouse effect is explored in detail for Northland in Laguë et al. (2021).

The colder climates seen in our simulations with extensive tropical land cover may resemble Snowball Earth conditions, when tropical oceans were hidden beneath sea glaciers (Hoffman et al. 1998), or during past geological epochs when land was clustered into large tropical supercontinents (Chandler et al. 1992; Merdith et al. 2021). Though not explored here, we note that differences in ocean dynamics on paleoclimate timescales can also be large drivers of differences in climate even with approximately similar continental configurations (Chiang 2009).

In addition to their dry atmospheres, the atmospheric circulations of LandWorld, TropicsLand, and NorthLand differ drastically from those of the other continental configurations. The meridional streamfunctions of the other continental configurations qualitatively resemble those of the modern Earth (Fig. 8). However, for LandWorld, TropicsLand, and NorthLand, the dry tropical landmasses are highly depleted of soil moisture, and as such the tropical Hadley circulation is not dominated by moist dynamics, but rather by dry convection. The result is an overturning circulation which is vertically very short, and resembles the Hadley circulation expected for Snowball Earth (Voigt et al. 2012; Voigt 2013) or the shallow meridional circulations over deserts (Zhai and Boos 2017). In the case of NorthLand, this only applies to the northern hemisphere.

3.6 Land heat capacity drives a seasonally asymmetric feedback with evaporation and water vapor

In this section, we focus on the differences between CapLand and Aqua, to explain why a planet that is 50% land covered is warmer and has more atmospheric water vapor than an aquaplanet where the entire planetary surface is ocean. The open tropical oceans in Aqua and CapLand result in these two simulations experiencing the most total evaporation and atmospheric water vapor of all our simulations (Figs. 4, 5). Note that in terms of global mean surface temperature, these simulations are the closest analogs to RealLand, which also has high surface evaporation and total atmospheric water vapor compared to other continental configurations.

The dark tropical ocean surface with effectively unlimited water for evaporation results in a moist tropical atmosphere for both CapLand and Aqua. Initially, water evaporated over the lower latitude ocean falls as precipitation on the equatorial edge of the polar continents of CapLand before it is evaporated again and transported by transient eddies to higher latitudes. Atmospheric moisture transport in CapLand provides enough water to maintain high soil moisture all year long (Figs. 7 and 18). We note, however, that both CapLand and Aqua experience temperatures below freezing at the high latitudes during winter (Fig. 15), and thus

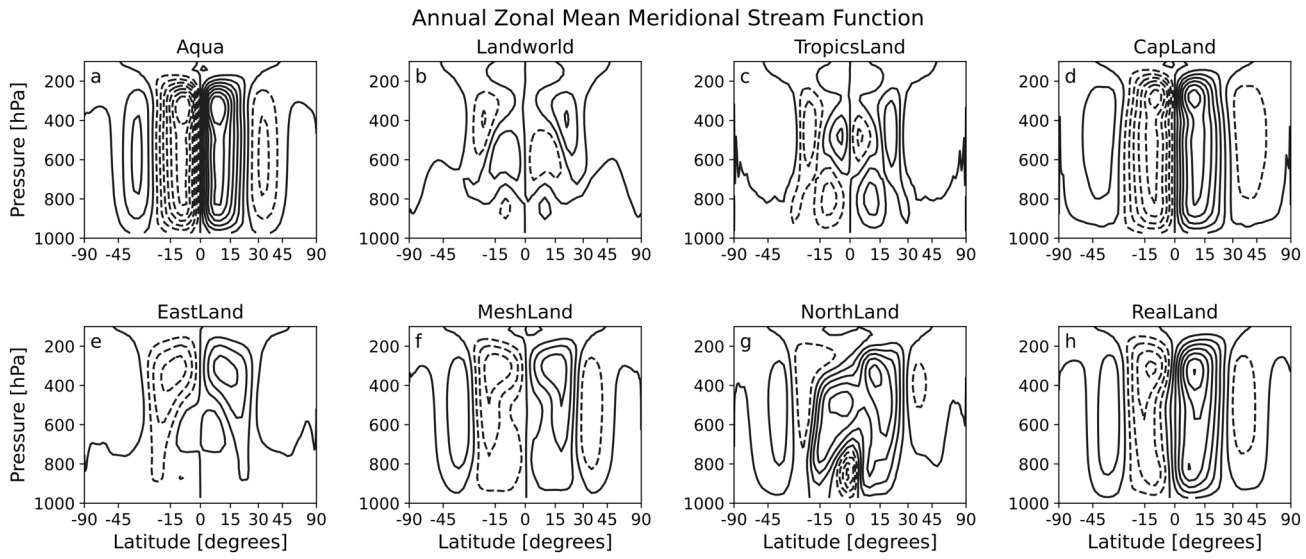

Fig. 8 Zonal mean meridional stream function annually averaged) for each continental configuration. Contours are spaced at 0.2×10^{11} kg/s. Solid contours indicate positive values (clockwise flow in this view) while dashed contours indicated negative values (counterclockwise flow)

we would expect the surface to be frozen for part of the year—but these simplified simulations do not account for the effects of sea ice or snow.

Despite its greater amount of land surface, CapLand is both warmer and has more atmospheric water vapor at all latitudes than Aqua (Fig. 9). This is particularly evident in the higher latitudes at higher levels of the troposphere, where the atmosphere in CapLand has over 100%—and in places in excess of 500%—more water vapor (in terms of specific humidity) than Aqua. While high soil moisture on the CapLand continents allows the surface to supply water to the atmosphere, the CapLand continent still differs from the high latitude ocean in Aqua in that it is brighter (higher albedo) and has a lower heat capacity.

The difference in both mean annual temperature and water vapor can be explained by the increased variation of seasonal temperature due to the land's lower heat capacity and a seasonal feedback through water vapor. Over land, the smaller heat capacity results in a larger seasonal amplitude of temperature than over ocean. CapLand has seasonally warmer local summers and cooler winters over the polar continent than over the oceans at the same latitude in Aqua (Fig. 10c, d). This increase in amplitude is expected; however, an increase in the annual mean temperature is not.

To explain the observed increase in mean temperature, we must consider two factors: (i) energy can be shed from the land surface not only as longwave radiation (LW), but also as sensible heat (SH) or evaporation/latent heat (LH), and (ii) feedbacks due to water vapor through the greenhouse effect and atmospheric energy transport. The seasonal imbalance between the local winter and summer is a result of a feedback between surface evaporation and the water vapor greenhouse effect.

During local summer, there is an increase in the total amount of radiative energy flowing into the land surface (SW + LW) in CapLand (Fig. 11a–c). This energy is shed from the land surface through a combination of increased surface temperatures (as evident by increased $LW^{\uparrow}$ and SH), and increased surface evaporation (Fig. 11d–f). This leads to more atmospheric water vapor; because of the nonlinearity of the Clausius Clapeyron relationship, the summer increase in specific humidity has a larger magnitude than the winter decrease (Fig. 9). Due to the increase in atmospheric water vapor during local summer, less incoming

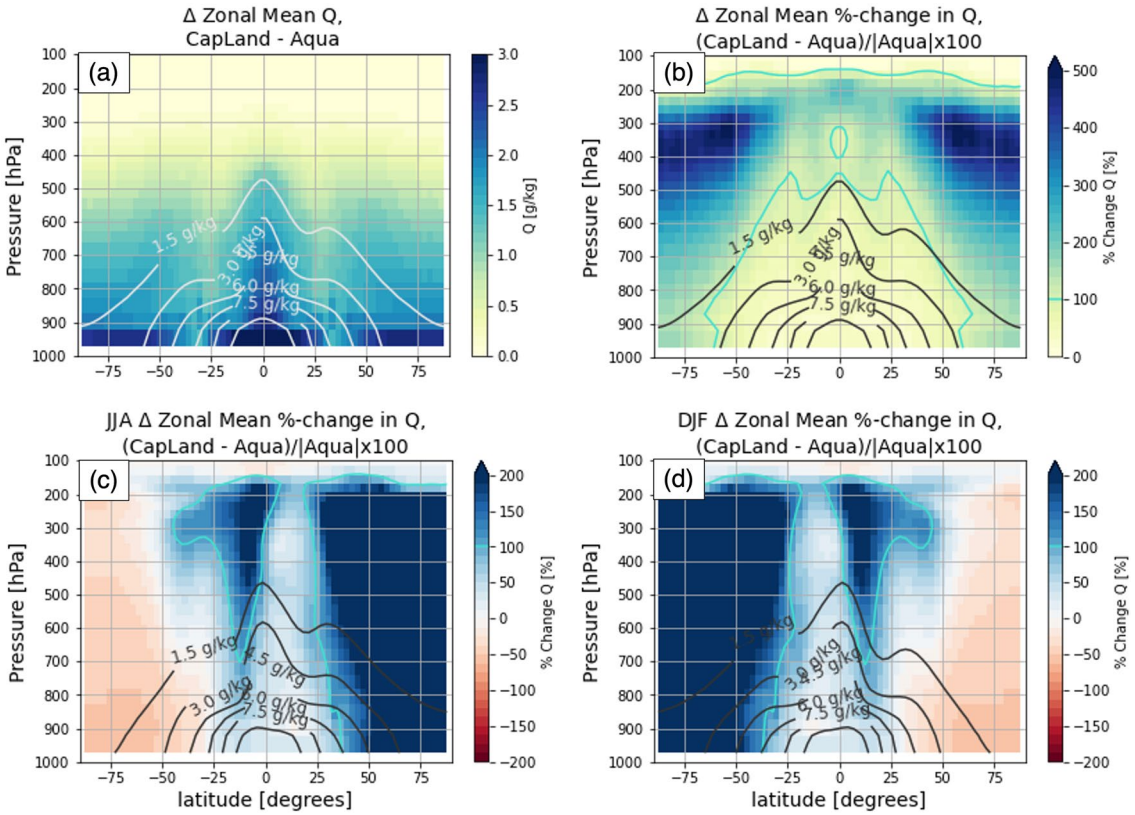

Fig. 9 Difference (CapLand—Aqua) in zonally averaged **a** annual mean specific humidity [g/kg] is shown in shading, with the climatological specific humidity [g/kg] from Aqua show in white contours. (b-c) show the percent change specific humidity for **b** the annual mean, **c** DJF, and **d** JJA in shading, with black contours showing climatological specific humidity [g/kg] from Aqua. Cyan contours in **b**–**d** show the 100% change in specific humidity line

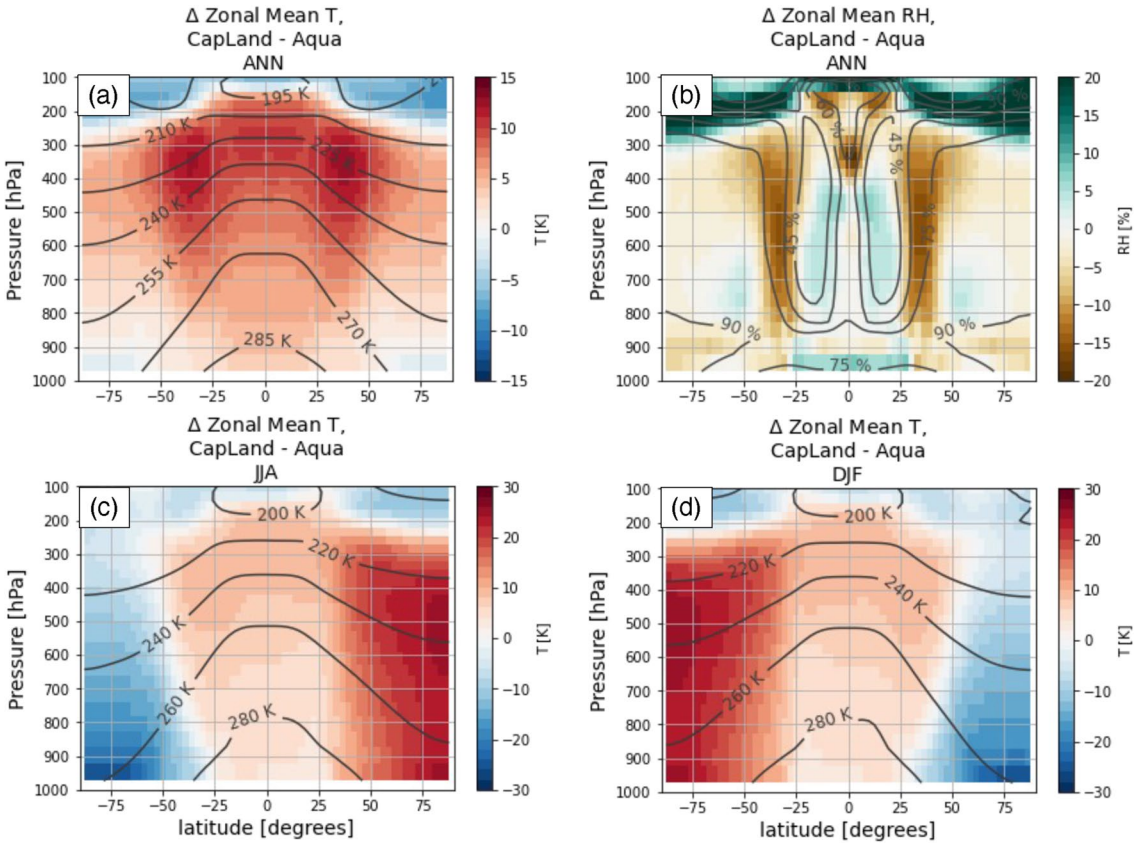

Fig. 10 Difference (CapLand—Aqua) in zonally averaged **a** annual mean air temperatures, **b** annual mean relative humidity, **c** DJF air temperatures and **d** JJA air temperatures, from the surface to 100 hPa. Contours show the climatological values for each field from the Aqua simulation

shortwave radiation reaches the surface (Fig. 11b). However, the increase in $LW^{\downarrow}$ into the surface is much larger than this decrease in $SW^{\downarrow}$ (Fig. 11a–c). The increase in $LW^{\downarrow}$ is a result of higher atmospheric temperatures and increased atmospheric water vapor, leading to a stronger greenhouse effect (which also helps to increase atmospheric temperatures).

Increased $LW^{\downarrow}$ into the surface adds energy into the land system, increasing the energy available for evaporation from the land. In CapLand, the soils remain wet through the summer (because of atmospheric moisture transport onto the continent; Figs. 7 and 18), supplying water to the hotter atmosphere and completing the feedback loop.

This evaporation-water vapor-greenhouse feedback is only possible *because* the continent in CapLand is very moist. Without available water on the polar continents, the small heat capacity of land would lead to warming but no change in evaporation rates in summer. In this hypothetical dry polar land scenario, the water vapor–greenhouse feedback would be much weaker or would not occur at all. The moist polar continents buffer the summer surface temperature response as excess energy from the strengthened greenhouse effect goes into evaporating more water rather than into warming the surface, which further strengthens the greenhouse effect. There is very little change in sensible heat flux at the surface between CapLand and Aqua, except right along the continental boundary (Fig. 11e).

The increased energy into the surface, increased evaporation, stronger water vapor greenhouse effect, and the resulting increase in energy into the surface are specific to summer, and create a seasonal imbalance in atmospheric air temperatures and atmospheric water vapor between summer and winter on CapLand vs. Aqua. The atmosphere over the continent in CapLand during local winter is slightly drier than the atmosphere over Aqua's ocean at the same latitude. In contrast, during local summer the atmosphere over CapLand is much more humid than the atmosphere over Aqua's ocean at the same latitude (Fig. 10). Concurrently, the magnitude of warming in summer is larger throughout the atmospheric column than the magnitude of cooling in winter. Only at low altitudes above the land surface is the winter cooling comparable to the summer warming in CapLand vs. Aqua (Figs. 10, 11f). The small heat capacity of land interacting with the seasonal cycle drives this feedback, which is why

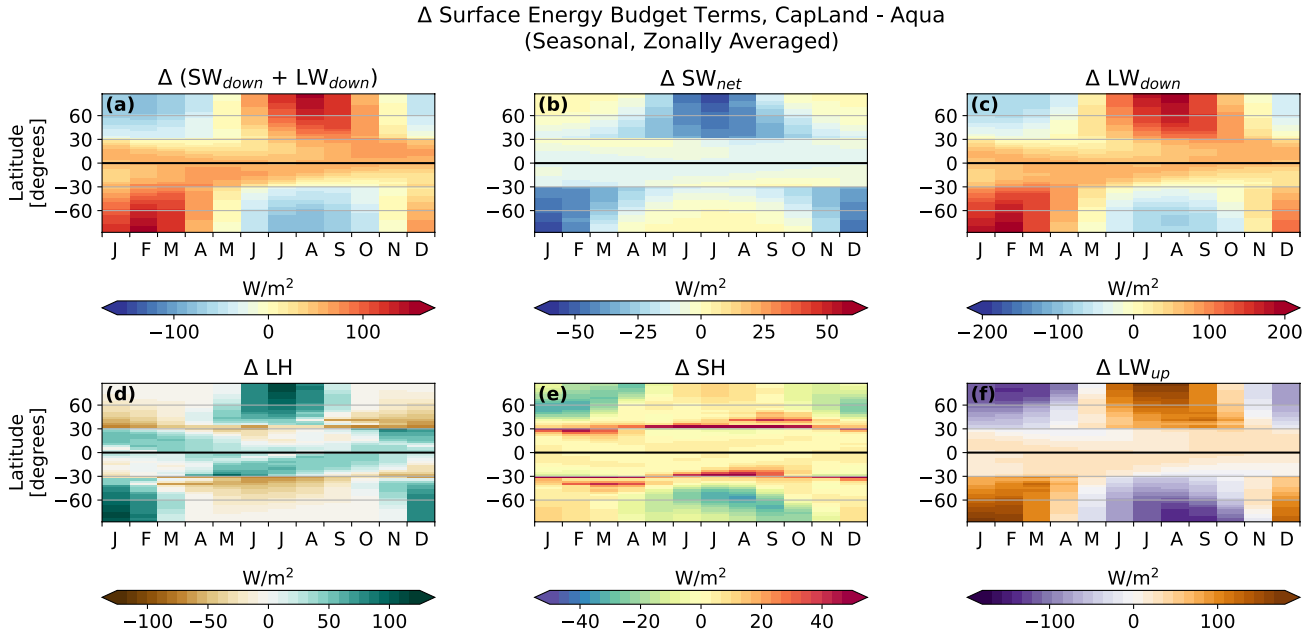

Fig. 11 Hovmoller plots showing the seasonal cycle of the difference in zonally averaged surface energy fluxes between CapLand and Aqua. The total radiative energy flux into the surface is shown in **a**, separated into the net absorbed SW in **b** and the downwelling LW in **c**. Panels **d**–**f** show the fluxes of energy leaving the surface, as latent heat flux (evaporation) in **d**, sensible heat flux in **e**, and emitted longwave radiation in **f**. Note the difference in the scale of the color bars between panels

summer temperatures are amplified in CapLand vs. in Aqua. This summertime CapLand-specific feedback does not occur in winter because evaporation is low in both CapLand and Aqua.

The non-linear relationship between longwave radiation and surface temperature could also introduce seasonally asymmetric temperature responses, however in our simulations, this relationship fails to explain our results. If we were to assume that the difference in insolation between summer and winter must be removed from the land surface as longwave radiation through a change in surface temperature (i.e. ignoring sensible or latent heat flux) and that the change in insolation is equal and opposite in summer vs. winter, then by the Stefan-Boltzmann law ($LW \propto \sigma T^4$; Stefan 1879), a *larger* change in surface temperature is needed during the cold season than is needed during the warm season in order to produce the same anomalous magnitude of longwave radiation. However, we do not find this in our simulations (Fig. 10c, d). Moreover, the critical difference in the CapLand vs. Aqua climate at high latitudes is the amplified amount of energy into the CapLand surface during local summer.

Past studies have explored similar idealized continental configurations to CapLand and TropicsLand, with opposing conclusions on which configuration makes for the warmer planet. Worsley and Kidder (1991) found that the tropical continental configuration allows for greater removal of CO_2 from the atmosphere through weathering and thus results in a cooler climate due to a diminished greenhouse effect. In contrast, Barron et al. (1984) found the polar continental configuration generates the cooler climate as it provides a surface for high-latitude snow accumulation, which generates cooling through snow albedo feedbacks. In this study, we identify a third mechanism of importance: the planet with moist land capping the poles and a tropical ocean is warmer than the planet with a tropical land belt and polar oceans because the continental arrangement exerts strong controls on evaporation and atmospheric water vapor.

A critical difference between our simulations and those of Barron et al. (1984) and Worsley and Kidder (1991) is our inclusion of a seasonal cycle. Without seasonality, the low heat capacity of land and the resulting summertime evaporation-water vapor-greenhouse effect feedback does not occur; this summertime warming feedback is the primary driver for our warmer CapLand simulation compared to Aqua. Moreover, our simulations do not allow for changing albedo from clouds, snow, or sea ice, nor changes in CO_2 due to weathering. Macdonald et al. (2019) find arc-continent collisions in the low latitudes increase the removal of atmospheric CO_2 through intensified chemical weathering, a similar mechanism to that invoked by Worsley and Kidder (1991). However, the weathering mechanism requires the tropical continent to receive adequate moisture to allow for rock weathering. Yet our TropicsLand simulation provides a potential counterexample to this, where a large tropical land mass could have low weathering rates due to the dry atmosphere with limited

precipitation. While we do not simulate rock weathering impacts on atmospheric CO_2 in our simulations, we would expect weathering rates to be lower over TropicsLand than, for example, MeshLand, which has much higher precipitation rates over land. That is, the intensity of weathering in the low latitudes requires not only the presence of land, but also the presence of precipitation. However, if our tropical continent were smaller in extent, allowing for more atmospheric water vapor and precipitation, the potential for CO_2 removal from rock weathering would likely be higher.

4 Conclusions

The distribution of land exerts a first-order control on global climate by modulating atmospheric water vapor concentrations. The eight idealized continental configurations considered here produced climates that span a range of roughly 15 K in global mean surface temperatures. We find strong relationships between surface evaporation, surface temperatures, and total atmospheric water vapor across the simulations.

While the climate of each continental configuration considered here differs, the mechanisms controlling these climates share many commonalities; in particular, each includes a feedback with the greenhouse effect of water vapor. When large landmasses are positioned in high insolation areas like the tropics, as is the case with TropicsLand, LandWorld, NorthLand, and EastLand, we do not get hot desert worlds; instead, the relatively dry land leads to water vapor depletion and a relatively cool climate. Our modern continental configuration drives a climate that is among the warmest and wettest of the configurations explored here, which is consistent with our findings that continental configurations with large tropical ocean area have warm, moist atmospheres. While there is land at low latitudes on modern Earth, there is also extensive ocean area; the relatively wet atmosphere of RealLand suggests that the modern Earth continental configuration does not limit tropical evaporation or tropical atmospheric water vapor.

Also of great importance is the fact that the low heat capacity of a wet continent at the poles in CapLand creates a larger seasonal cycle of temperature and generates a seasonal evaporation/water vapor feedback that amplifies summer warming. This feedback creates a climate that is wetter and warmer on a planet with 50% land cover than on an aquaplanet without continents.

Our framework allows us to isolate a new mechanism through which tropical vs. extratropical land masses can modulate global-scale climate, and also highlights the importance of continental distribution for global climate through its influence on atmospheric water vapor. Further study is required to determine the combined climate effects of tropical vs. extratropical land on long-term atmospheric CO_2 concentrations, surface albedo (through snow cover), and top-of-atmosphere albedo (through cloud cover and water vapor effects). How much these various effects may amplify, damp, or generate interactions which could further feed back on global climate is necessary to understand the total impact of continental distribution on global-scale climate.

The different continental configurations explored here are idealizations, but provide possible analogues for past continental configurations (see Merdith et al. 2021), or configurations on different water-land planets. We show how the distribution of land on a planet's surface has a fundamental control on surface climate by modulating atmospheric water vapor concentrations and creating feedbacks between heat capacity and the seasonal cycle, with variations in the distribution of a fixed amount of land across the planetary surface generating a substantial spread in global mean surface climate.

Appendix A: Spinup and additional fields of interest

See Figs. 12, 13 and 14.

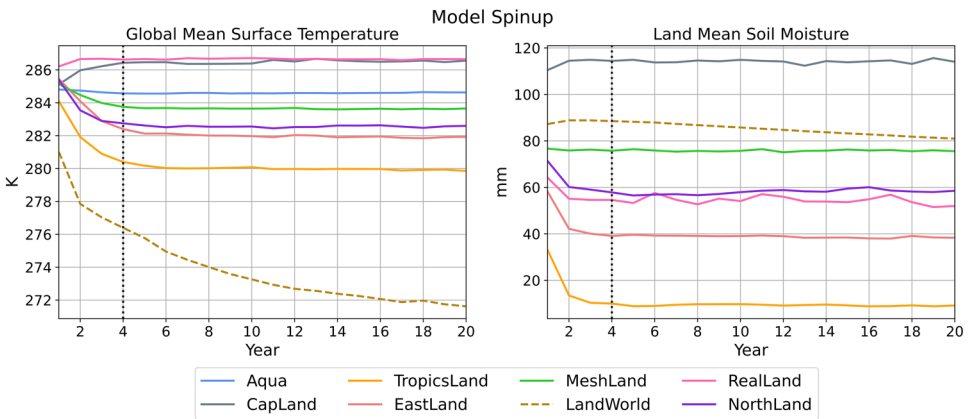

Fig. 12 Annual mean **a** global-mean surface temperature [K] and **b** land-mean soil moisture (water in soil "bucket", in [mm]) for each model simulation, showing equilibration within 4 years of initialization for all simulations except LandWorld (dashed tan line). The vertical dotted at year 4 marks the end of the spin-up period; model output up to and including year 4 are discarded from the analysis in this study

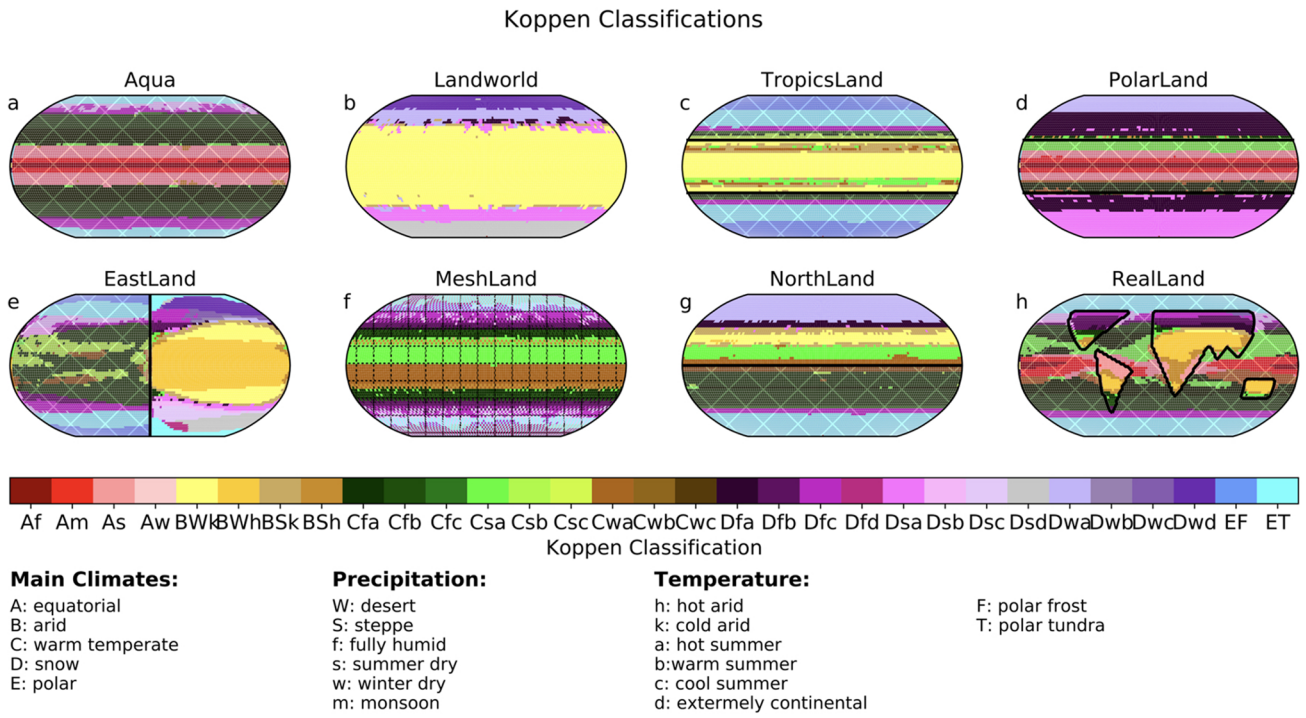

Fig. 13 Köppen–Geiger climate zones for each continental configuration, calculated following Kottek et al. (2006)

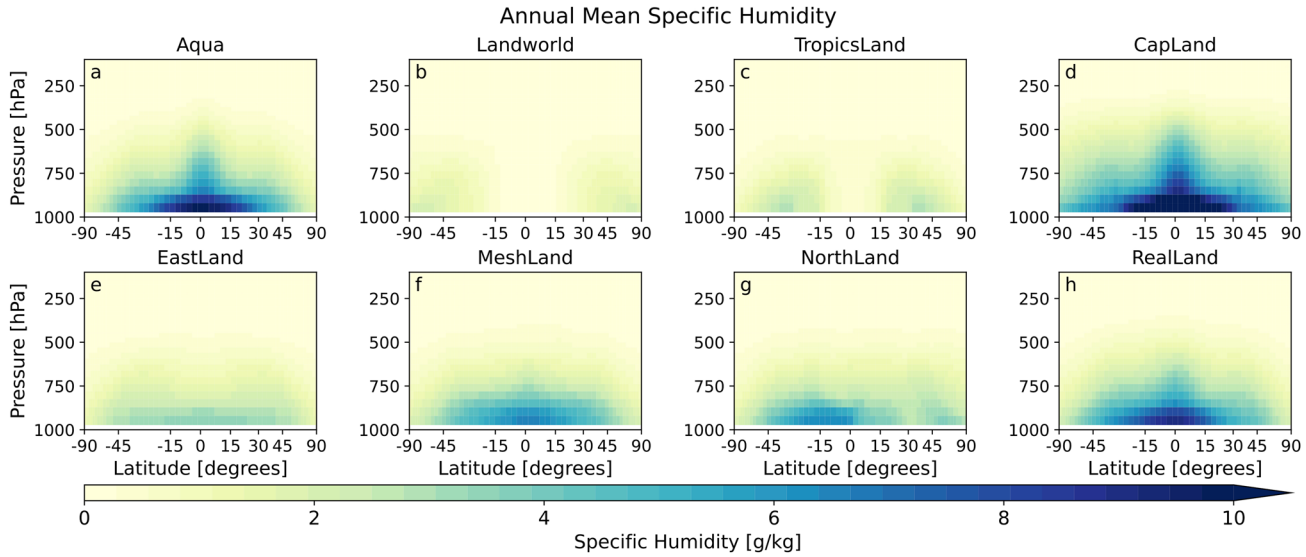

Fig. 14 Zonally averaged annual mean specific humidity from the surface to 100 hPa for each continental configuration

Appendix B Transient and seasonal adjustments

See Figs. 15, 16, 17 and 18.

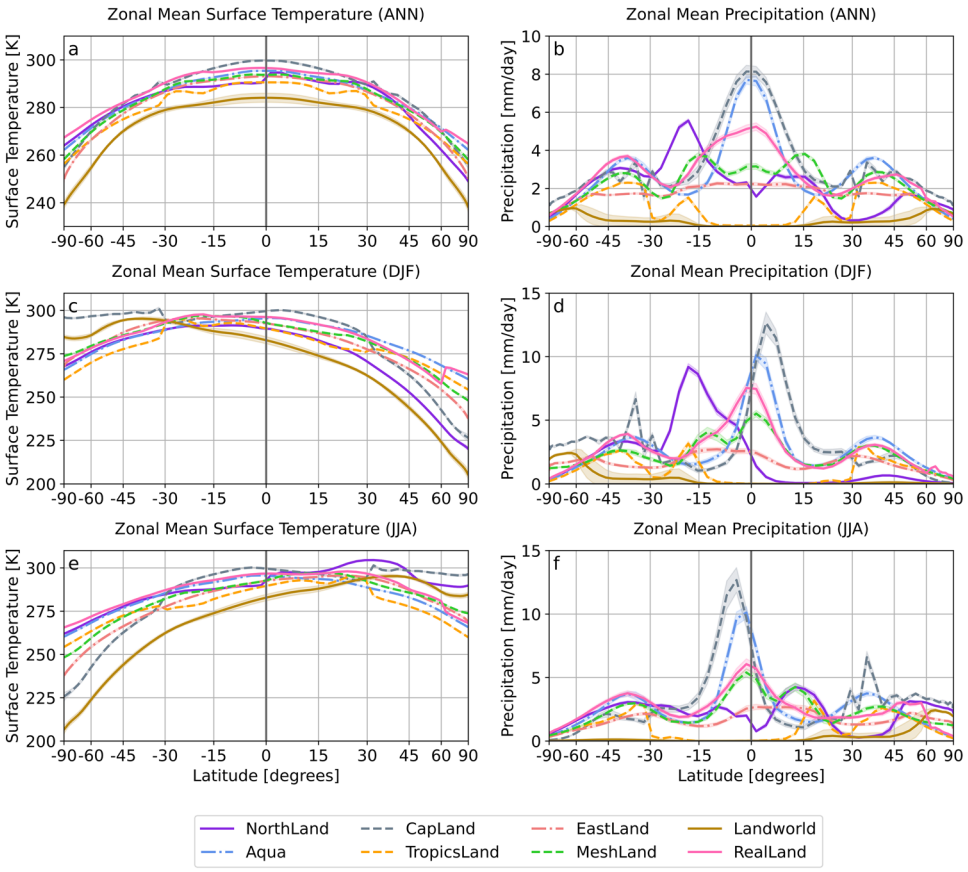

Fig. 15 Zonally averaged surface temperature (left) and precipitation (right) for each simulation in the annual mean (top), DJF (middle) and JJA (bottom)

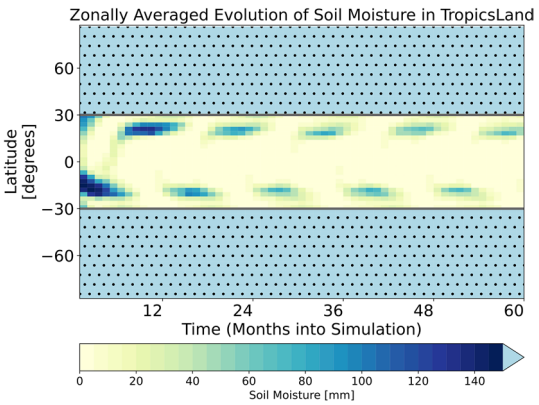

Fig. 16 Hovmoller plot showing the evolution of zonally averaged soil moisture for the first 5 years of the TropicsLand simulation [mm]. Ocean areas are indicated by light blue shading with stippling

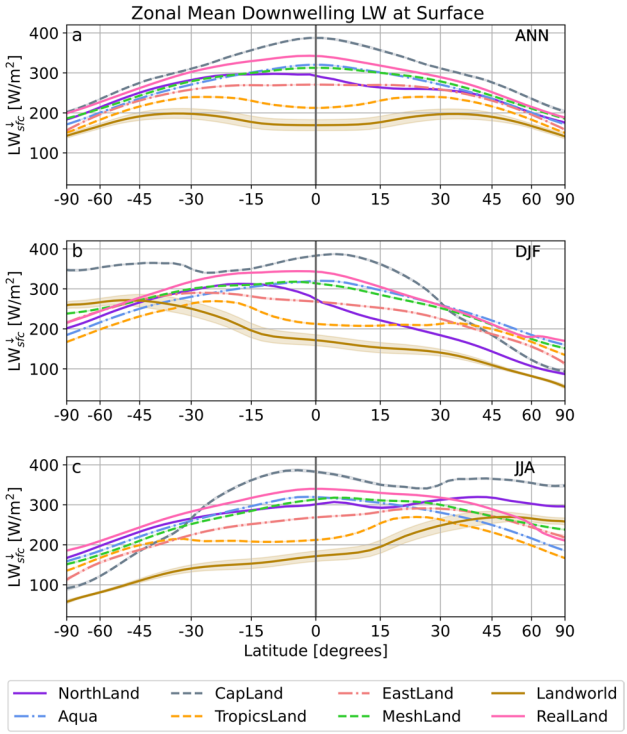

Fig. 17 Zonally averaged downwelling longwave radiation at the surface ($LW^{\downarrow}_{sfc}$, in W/m^2) for **a** the annual mean, **b** December–January–February, and **c** June–July–August for each continental configuration. Shading indicates $\pm 1\sigma$ of interannual variability

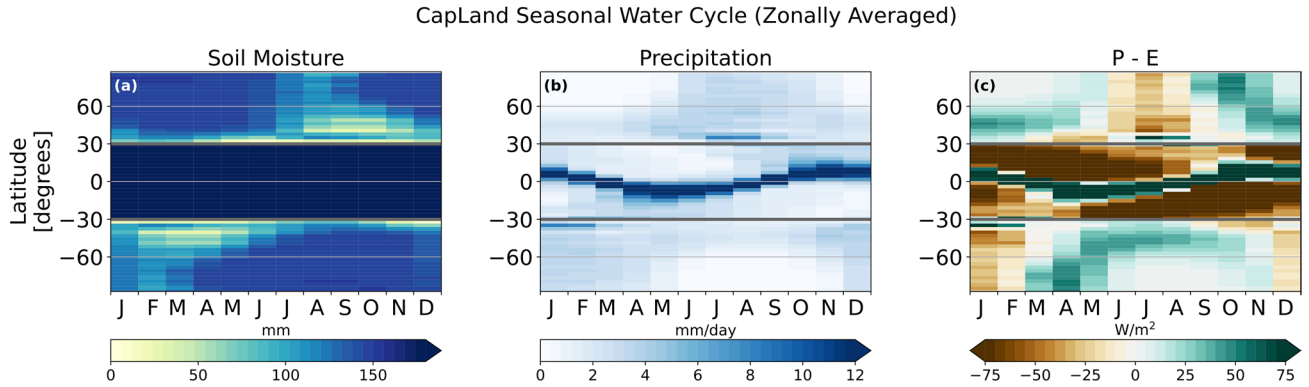

Fig. 18 Zonally averaged **a** soil moisture [mm], **b** precipitation [mm/day], and **c** precipitation-evaporation [W/m^2] over the course of the year for the CapLand simulation. Dark gray lines at 30° N/S indicate the continental/ocean boundary

Acknowledgements This research used the Savio computational cluster resource provided by the Berkeley Research Computing program at the University of California, Berkeley (supported by the UC Berkeley Chancellor, Vice Chancellor for Research, and Chief Information Officer). This research used resources of the National Energy Research Scientific Computing Center (NERSC), a U.S. Department of Energy Office of Science User Facility located at Lawrence Berkeley National Laboratory, operated under Contract No. DE-AC02-05CH11231. We acknowledge high-performance computing support for analysis using the Casper platform of Cheyenne (https://doi.org/10.5065/D6RX99HX) provided by NCAR's Computational and Information Systems Laboratory, sponsored by the National Science Foundation.

Author contributions MML designed the study, conducted the simulations, and conducted the analysis. MML and SR discussed the preliminary concept of the study. MML, GRQ, and WRB discussed results and further analysis. SR conducted the literature review. The first draft of the manuscript was written by MML and all authors contributed to and commented on intermediate versions of the manuscript. All authors read and approved the final manuscript.

Funding M.M.L. acknowledges funding support from the James S. McDonnell Foundation Postdoctoral Fellowship in Dynamic and Multiscale Systems. SR acknowledges support from NSF Award OCE-1850900.

Data availability Isca is publicly available on github at https://github.com/ExeClim/Isca. The specific version of Isca used in this study is archived on zenodo and github with the DOI https://doi.org/10.5281/zenodo.6800218. The analysis code, output from model simulations, python driver scripts, and modifications to the source code used in this study are publicly archived on zenodo with the DOIs https://doi.org/10.5281/zenodo.7964297 and https://doi.org/10.5281/zenodo.7754428.

Declarations

Conflict of interest The authors have no relevant financial or non-financial interests to disclose.

Ethical approval Not applicable.

References

Baldocchi DD, Vogel CA, Hall B (1997) Seasonal variation of energy and water vapor exchange rates above and below a boreal jack pine forest canopy generally less than one-half was wet, daily evaporation. J Geophys Res 102(96):28928–939951. https://doi.org/10.1029/96JD03325

Baross JA, Benner SA, Cody GD et al (2007) The limits of organic life in planetary systems. National Academies Press, Washington DC. https://doi.org/10.17226/11919

Barron EJ, Thompson SL, Hay WW (1984) Continental distribution as a forcing factor for global-scale temperature. Nature 310(5978):574–575. https://doi.org/10.1038/310574a0

Barsugli J, Shin SI, Sardeshmukh PD (2005) Tropical climate regimes and global climate sensitivity in a simple setting. J Atmos Sci 62(4):1226–1240. https://doi.org/10.1175/JAS3404.1

Betts AK (1986) A new convective adjustment scheme. Part I: observational and theoretical basis. Q J R Meteorol Soc 112(473):677–691. https://doi.org/10.1002/qj.49711247307

Betts AK, Miller MJ (1986) A new convective adjustment scheme. Part II: single column tests using GATE wave, BOMEX, ATEX and arctic air-mass data sets. Q J R Meteorol Soc 112(473):693–709. https://doi.org/10.1002/qj.49711247308

Bonan GB (2008) Forests and climate change: forcings, feedbacks, and the climate benefits of forests. Science (New York, NY) 320(5882):1444–1449. https://doi.org/10.1126/science.1155121

Budyko MI (1961) The heat balance of the earth's surface. Sov Geogr 2(4):3–13. https://doi.org/10.1080/00385417.1961.10770761

Budyko MI (1969) The effect of solar radiation variations on the climate of the Earth. Tellus 21(5):611–619. https://doi.org/10.3402/tellusa.v21i5.10109

Burke CJ, Christiansen JL, Mullally F et al (2015) Terrestrial planet occurrence rates for the Kepler GK dwarf sample. Astrophys J 809(1):8. https://doi.org/10.1088/0004-637X/809/1/8

Cess RD, Goldenberg SD (1981) The effect of ocean heat capacity upon global warming due to increasing atmospheric carbon dioxide. J Geophys Res 86(80):498–502

Chandler MA, Rind D, Ruedy R (1992) Pangaean climate during the early Jurassic: GCM simulations and the sedimentary record of paleoclimate. Geol Soc Am Bull 104(5):543–559. https://doi.org/10.1130/0016-7606(1992)104<0543:PCDTEJ>2.3.CO;2

Charney J, Stone PH, Quirk WJ (1975) Drought in Sahara—biogeophysical feedback mechanism. Science 187(4175):434–435. https://doi.org/10.1126/science.187.4175.434

Chiang JC (2009) The tropics in paleoclimate. Annu Rev Earth Planet Sci 37:263–297. https://doi.org/10.1146/annurev.earth.031208.100217

Cho MH, Yang AR, Baek EH et al (2018) Vegetation-cloud feedbacks to future vegetation changes in the Arctic regions. Clim Dyn 50(9–10):3745–3755. https://doi.org/10.1007/s00382-017-3840-5

Clough SA, Shephard MW, Mlawer EJ et al (2005) Atmospheric radiative transfer modeling: a summary of the AER codes. J Quant Spectrosc Radiat Transf 91(2):233–244. https://doi.org/10.1016/j.jqsrt.2004.05.058

Cronin TW, Emanuel KA, Molnar P (2015) Island precipitation enhancement and the diurnal cycle in radiative-convective equilibrium. Q J R Meteorol Soc 141(689):1017–1034. https://doi.org/10.1002/qj.2443

Davin EL, de Noblet-Ducoudré N, de Noblet-Ducoudre N et al (2010) Climatic impact of global-scale deforestation: radiative versus nonradiative processes. J Clim 23(1):97–112. https://doi.org/10.1175/2009JCLI3102.1

Dirmeyer PA (1998) Land-sea geometry and its effect on monsoon circulations. J Geophys Res Atmos 103(D10):11555–11572. https://doi.org/10.1029/98JD00802

Donohoe A, Battisti DS (2011) Atmospheric and surface contributions to planetary albedo. J Clim 24(16):4402–4418. https://doi.org/10.1175/2011JCLI3946.1

Donohoe A, Marshall J, Ferreira D et al (2013) The relationship between ITCZ location and cross-equatorial atmospheric heat transport: from the seasonal cycle to the Last Glacial Maximum. J Clim 26(11):3597–3618. https://doi.org/10.1175/JCLI-D-12-00467.1

Eliassen A, Palm E (1960) On the transfer of energy in stationary mountain waves. Geofysiske Publikasjoner

Enderton D, Marshall J (2009) Explorations of atmosphere–ocean–ice climates on an aquaplanet and their meridional energy transports. J Atmos Sci 66(6):1593–1611. https://doi.org/10.1175/2008JAS2680.1

Fajber R, Kushner PJ (2021) Using 'heat tagging' to understand the remote influence of atmospheric diabatic heating through long-range transport. J Atmos Sci. https://doi.org/10.1175/JAS-D-20-0290.1

Ferrari R, Ferreira D (2011) What processes drive the ocean heat transport? Ocean Modelling. https://doi.org/10.1016/j.ocemod.2011.02.013

Ferreira D, Marshall J, Campin JM (2010) Localization of deep water formation: role of atmospheric moisture transport and geometrical constraints on ocean circulation. J Clim 23(6):1456–1476. https://doi.org/10.1175/2009JCLI3197.1

Frierson DM (2007) The dynamics of idealized convection schemes and their effect on the zonally averaged tropical circulation. J Atmos Sci 64(6):1959–1974. https://doi.org/10.1175/JAS3935.1

Geen R, Lambert FH, Vallis GK (2018) Regime change behavior during Asian monsoon onset. J Clim 31(8):3327–3348. https://doi.org/10.1175/JCLI-D-17-0118.1

Harris CR, Millman KJ, van der Walt SJ et al (2020) Array programming with NumPy. Nature 585(7825):357–362. https://doi.org/10.1038/s41586-020-2649-2

Held IM (1985) Pseudomomentum and the orthogonality of modes in shear flows. J Atmos Sci 42(21):2280–2288. https://doi.org/10.1175/1520-0469(1985)042<2280:PATOOM>2.0.CO;2

Held IM, Ting M, Wang H (2002) Northern winter stationary waves: theory and modeling. J Clim 15(16):2125–2144. https://doi.org/10.1175/1520-0442(2002)015<2125:NWSWTA>2.0.CO;2

Herman GF, Wu MLC, Johnson WT (1980) The effect of clouds on the earth's solar and infrared radiation budgets. J Atmos Sci 37(June):1251–1261

Hoffman PF, Schrag DP (2002) The snowball Earth hypothesis: testing the limits of global change. Terra Nova 14(3):129–155. https://doi.org/10.1046/j.1365-3121.2002.00408.x

Hoffman PF, Kaufman AJ, Halverson GP et al (1998) A neoproterozoic snowball earth. Science 281(5381):1342–1346. https://doi.org/10.1126/science.281.5381.1342

Hoffman PF, Abbot DS, Ashkenazy Y et al (2017) Snowball Earth climate dynamics and Cryogenian geology-geobiology. Sci Adv 3(11). https://doi.org/10.1126/sciadv.1600983

Houze RA (2012) Orographic effects on precipitating clouds. Rev Geophys 50(1):1–47. https://doi.org/10.1029/2011RG000365

Hoyer S, Hamman J (2017) Xarray: N-D labeled arrays and datasets in Python. J Open Res Softw 5(1). https://doi.org/10.5334/jors.148

Hu S, Boos WR (2017) The physics of orographic elevated heating in radiative-convective equilibrium. J Atmos Sci 74(9):2949–2965. https://doi.org/10.1175/JAS-D-16-0312.1

Hui KL, Bordoni S (2021) Response of monsoon rainfall to changes in the latitude of the equatorward coastline of a zonally symmetric continent. J Atmos Sci 78(5):1429–1444. https://doi.org/10.1175/JAS-D-20-0110.1

IPCC (2013) Climate Change 2013. The physical change basis. Climate Change 2013: the physical science basis contribution of Working Group I to the fifth assessment report of the Intergovernmental Panel on Climate Change. https://doi.org/10.1017/CBO9781107415324

Jin Z, Charlock TP, Smith WL et al (2004) A parameterization of ocean surface albedo. Geophys Res Lett 31(22):1–4. https://doi.org/10.1029/2004GL021180

Kang SM, Held IM, Frierson DMW et al (2008) The response of the ITCZ to extratropical thermal forcing: idealized slab-ocean experiments with a GCM. J Clim 21(14):3521–3532. https://doi.org/10.1175/2007JCLI2146.1

Kang SM, Frierson DMW, Held IM (2009) The tropical response to extratropical thermal forcing in an idealized GCM: the importance of radiative feedbacks and convective parameterization. J Atmos Sci 66(9):2812–2827. https://doi.org/10.1175/2009JAS2924.1

Khanna J, Medvigy D (2014) Strong control of surface roughness variations on the simulated dry season regional atmospheric response to contemporary deforestation in Rondonia, Brazil. J Geophys Res D Atmos 119(23):13067–13078. https://doi.org/10.1002/2014JD022278

Kiehl JT, Trenberth KE (1997) Earth's annual global mean energy budget. Bull Am Meteorol Soc 78(2):197–208

Kim JE, Laguë MM, Pennypacker S et al (2020) Evaporative resistance is of equal importance as surface albedo in high-latitude surface temperatures due to cloud feedbacks. Geophys Res Lett 47(4). https://doi.org/10.1029/2019GL085663

Kirshbaum DJ, Smith RB (2009) Orographic precipitation in the tropics: large-Eddy simulations and theory. J Atmos Sci 66(9):2559–2578. https://doi.org/10.1175/2009JAS2990.1

Kirtman BP, Shukla J (2000) Influence of the Indian summer monsoon on ENSO. Q J R Meteorol Soc 126(562):213–239. https://doi.org/10.1002/qj.49712656211

Kite ES, Ford EB (2018) Habitability of exoplanet waterworlds. Astrophys J 864(1):75. https://doi.org/10.3847/1538-4357/aad6e0

Knippertz P, Wernli H (2010) A Lagrangian climatology of tropical moisture exports to the northern hemispheric extratropics. J Clim 23(4):987–1003. https://doi.org/10.1175/2009JCLI3333.1

Kooperman GJ, Chen Y, Hoffman FM et al (2017) Forest response to rising CO_2 drives zonally asymmetric rainfall change over tropical continents. Nat Clim Change 8(5):1–36. https://doi.org/10.1038/s41558-018-0144-7

Kottek M, Grieser J, Beck C et al (2006) World map of the Köppen–Geiger climate classification updated. Meteorol Z 15(3):259–263. https://doi.org/10.1127/0941-2948/2006/0130

Laguë MM, Bonan GB, Swann ALS (2019) Separating the impact of individual land surface properties on the terrestrial surface energy budget in both the coupled and uncoupled land-atmosphere system. J Clim 32(18):5725–5744. https://doi.org/10.1175/jcli-d-18-0812.1

Laguë MM, Pietschnig M, Ragen S et al (2021) Terrestrial evaporation and global climate: lessons from Northland, a planet with a hemispheric continent. J Clim 34(6):2253–2276. https://doi.org/10.1175/jcli-d-20-0452.1

Loft G (1918) The Gulf Stream and the North Atlantic Drift. J Geogr 17(1):8–17. https://doi.org/10.1080/00221341808984367

Macdonald FA, Swanson-hysell NL, Park Y et al (2019) Arc-continent collisions in the tropics set Earth's climate state. Science 184(April):181–184

Manabe S (1969) Climate and the ocean circulation. Mon Weather Rev 97(11):739–774. https://doi.org/10.1175/1520-0493(1969)097<0739:CATOC>2.3.CO;2

Manabe S, Terpstra TB (1974) The effect of mountains on the general circulation of the atmosphere. J Atmos Sci 31(1):3

Maroon EA, Frierson DM (2016) The impact of a continent's longitudinal extent on tropical precipitation. Geophys Res Lett 43(22):11921–11929. https://doi.org/10.1002/2016GL071518

Maroon EA, Frierson DM, Battisti DS (2015) The tropical precipitation response to Andes topography and ocean heat fluxes in an aquaplanet model. J Clim 28(1):381–398. https://doi.org/10.1175/JCLI-D-14-00188.1

McFarlane NA (1987) The effect of orographically excited gravity wave drag on the general circulation of the lower stratosphere and troposphere. J Atmos Sci 44(14):1775–1800. https://doi.org/10.1175/1520-0469(1987)044<1775:teoeog>2.0.co;2

Méndez A, Rivera-Valentín EG, Schulze-Makuch D et al (2021) Habitability models for astrobiology. Astrobiology 21(8):1017–1027. https://doi.org/10.1089/ast.2020.2342

Merdith AS, Williams SE, Collins AS et al (2021) Extending full-plate tectonic models into deep time: linking the Neoproterozoic and the Phanerozoic. Earth Sci Rev 214:103477. https://doi.org/10.1016/j.earscirev.2020.103477

Mlawer EJ, Taubman SJ, Brown PD et al (1997) Radiative transfer for inhomogeneous atmospheres: RRTM, a validated correlated-k model for the longwave. J Geophys Res Atmos 102(D14):16663–16682. https://doi.org/10.1029/97JD00237

North GR, Mengel JG, Short DA (1983) Simple energy balance model resolving the seasons and the continents: application to the astronomical theory of the ice ages. J Geophys Res 88(C11):6576–6586. https://doi.org/10.1029/JC088iC11p06576

Payne RE (1972) Albedo of the sea surface. J Atmos Sci 29(5):959–970. https://doi.org/10.1175/1520-0469(1972)029<0959:aotss>2.0.co;2

Penn JL, Deutsch C, Payne JL et al (2018) Temperature-dependent hypoxia explains biogeography and severity of end-Permian marine mass extinction. Science 362(6419). https://doi.org/10.1126/science.aat1327

Pierrehumbert RT (2010) Principles of planetary climate, 1st edn. Cambridge University Press, Cambridge. https://doi.org/10.1017/CBO9780511780783

Pietschnig M, Swann AL, Lambert FH et al (2021) Response of tropical rainfall to reduced evapotranspiration depends on continental extent. J Clim 34(23):9221–9234. https://doi.org/10.1175/JCLI-D-21-0195.1

Queney P (1948) The problem of air flow over mountains: a summary of theoretical studies. Bull Am Meteorol Soc 29(1):16–26. https://doi.org/10.1175/1520-0477-29.1.16

Richardson PL (1980) Benjamin Franklin and Timothy Folger's first printed chart of the gulf stream. Science 207(4431):643–645

Rushby AJ, Shields AL, Wolf ET et al (2020) The effect of land albedo on the climate of land-dominated planets in the TRAPPIST-1 system. Astrophys J 904(2):124. https://doi.org/10.3847/1538-4357/abbe04

Salem BBC (1989) Arid zone forestry: a guide for field technicians. FAO Conservation Guide No. 20

Saulière J, Brayshaw DJ, Hoskins B et al (2012) Further investigation of the impact of idealized continents and SST distributions on the northern hemisphere storm tracks. J Atmos Sci 69(3):840–856. https://doi.org/10.1175/JAS-D-11-0113.1

Seager S (2013) Exoplanet habitability. Astrophys J 340(May):577–582. https://doi.org/10.1088/0004-637X/777/2/95

Shukla J, Mintz Y (1982) Influence of land-surface evapotranspiration on the earth's climate. Science 215(4539):1498–1501. https://doi.org/10.1126/science.215.4539.1498

Sikma M, Vilà-Guerau de Arellano J (2019) Substantial reductions in cloud cover and moisture transport by dynamic plant responses. Geophys Res Lett 46(3):1870–1878. https://doi.org/10.1029/2018GL081236

Stefan J (1879) On the relationship between thermal radiation and temperature. Bull Sess Vienna Acad Sci (Vienna, 1879) 79:391–428

Stone PH (1978) Baroclinic adjustment. J Atmos Sci 35(April):561–571

Straume EO, Gaina C, Medvedev S et al (2020) Global Cenozoic Paleobathymetry with a focus on the Northern Hemisphere Oceanic Gateways. Gondwana Res 86:126–143. https://doi.org/10.1016/j.gr.2020.05.011

Sud YC, Shukla J, Mintz Y (1988) Influence of land surface roughness on atmospheric circulation and precipitation: a sensitivity study with a general circulation model. J Appl Meteorol 27(9):1036–1054. https://doi.org/10.1175/1520-0450(1988)027<1036:iolsro>2.0.co;2

Thomson SI, Vallis GK (2019) Hierarchical modeling of solar system planets with Isca. Atmosphere 10(12):1–21. https://doi.org/10.3390/ATMOS10120803

Tierney JE, Poulsen CJ, Montañez IP et al (2020) Past climates inform our future. Science 370(6517):eaay3701. https://doi.org/10.1126/science.aay3701

Vallis GK, Colyer G, Geen R et al (2018) Isca, v1.0: a framework for the global modelling of the atmospheres of Earth and other planets at varying levels of complexity. Geosci Model Dev 11(3):843–859. https://doi.org/10.5194/gmd-11-843-2018

Van Rossum G, Drake FL (2009) Python 3 Reference Manual. CreateSpace, Scotts Valley. https://doi.org/10.5555/1593511

Virtanen P, Gommers R, Oliphant TE et al (2020) SciPy 1.0: fundamental algorithms for scientific computing in Python. Nat Methods 17(3):261–272. https://doi.org/10.1038/s41592-019-0686-2

Voigt A (2013) The dynamics of the Snowball Earth Hadley circulation for off-equatorial and seasonally varying insolation. Earth Syst Dyn 4(2):425–438. https://doi.org/10.5194/esd-4-425-2013

Voigt A, Held IM, Marotzke J (2012) Hadley cell dynamics in a virtually dry snowball Earth atmosphere. J Atmos Sci 69(1):116–128. https://doi.org/10.1175/JAS-D-11-083.1

Voigt A, Bony S, Dufresne JL et al (2014) The radiative impact of clouds on the shift of the Intertropical Convergence Zone. Geophys Res Lett 41(12):4308–4315. https://doi.org/10.1002/2014GL060354

Voosen P (2019) A 500-million-year survey of Earth's climate reveals dire warning for humanity. Science. https://doi.org/10.1126/science.aay1323

White RH, Battisti DS, Roe GH (2017) Mongolian mountains matter most: impacts of the latitude and height of Asian orography on pacific wintertime atmospheric circulation. J Clim 30(11):4065–4082. https://doi.org/10.1175/JCLI-D-16-0401.1

Wiscombe W, Warren S (1980) A model for spectral Albedo I: pure snow

Worsley TR, Kidder DL (1991) First-order coupling of paleogeography and CO_2, with global surface temperature and its latitudinal contrast. Geology 19(12):1161–1164. https://doi.org/10.1130/0091-7613(1991)019<1161:FOCOPA>2.3.CO;2

Yasunari T, Saito K, Takata K (2006) Relative roles of large-scale orography and land surface processes in the global hydroclimate. Part I: impacts on monsoon systems and the tropics. J Hydrometeorol 7(4):626–641. https://doi.org/10.1175/JHM515.1

Zelinka MD, Randall DA, Webb MJ et al (2017) Clearing clouds of uncertainty. Nat Clim Change 7(10):674–678. https://doi.org/10.1038/nclimate3402

Zhai J, Boos WR (2017) The drying tendency of shallow meridional circulations in monsoons. Q J R Meteorol Soc 143(708):2655–2664. https://doi.org/10.1002/qj.3091

Zhou W, Xie SP (2018) A hierarchy of idealized monsoons in an intermediate GCM. J Clim 31(22):9021–9036. https://doi.org/10.1175/JCLI-D-18-0084.1